DIRECT ENERGY CONVERSION USING THE BETA-VOLTAIC EFFECT IN EPITAXIAL SILICON P-N JUNCTION DEVICES

DIRECT ENERGY CONVERSION USING THE BETA-VOLTAIC EFFECT IN EPITAXIAL SILICON P-N JUNCTION DEVICES

by

R. Keeffe, B.Sc.

A Thesis

Submitted to the School of Graduate Studies

in Partial Fulfilment of the Requirements

for the Degree

Master of Science

McMaster University

September, 1973

MASTER OF SCIENCE (1973) McMASTER UNIVERSITY

(Materials Science) Hamilton, Ontario

TITLE: Direct Energy Conversion Using the Beta-Voltaic Effect in Epitaxial Silicon P-N Junction Devices

AUTHOR: Richard Keeffe, B.Sc. (Saint Francis Xavier University)

SUPERVISOR: Dr. J. Shewchun, Engineering Physics

NUMBER OF PAGES: x, 106

ABSTRACT

This thesis presents an investigation of the electron-voltaic effect using epitaxial P-N junctions. The effect is manifested in the direct energy conversion of beta particles emitted from a radioisotope promethium^{147} source by single and multi-junction devices. The purpose of the investigation is to determine the power outputs of the devices which may be combined in series and parallel combinations in the construction of an atomic battery with a small size and long lifetime (approximately 5 - 10 years).

ACKNOWLEDGMENTS

I wish to express my appreciation to Dr. John Shewchun for his support in this work. I would also like to thank Martin Green, Dave King and Lawrence Gooderich for many helpful discussions. The loan of equipment from Canadian Westinghouse in profiling my devices is gratefully acknowledged. Finally, I would like to thank Lydea de Jong for typing the manuscript and Atomic Energy of Canada for their financial assistance.

TABLE OF CONTENTS

LIST OF FIGURES

LIST OF TABLES

CHAPTER I

INTRODUCTION

An energy converting electrical power source can be constructed by exposing a P-N junction to radiation (optical or nuclear). The incident radiation produces electron-hole pairs by collision or photo-excitation. The electrons and holes which are within a diffusion length of the junction may then diffuse to the junction. Upon reaching the junction the electrons from the p-type side descend the potential barrier into the n-type region while the holes from the n-type region cross the junction into the p-type side. By crossing the junction both the electrons and holes reduce their potential energy. Because of the change in carrier concentration near the junction the potential barrier is reduced when a load is applied to the terminals of the irradiated device and the P-N junction is effectively forward biased. The biased junction acts as a battery and can deliver power to the load. In the case of beta emitting nuclear sources each high energy beta particle produces many electron-hole pairs at low energy, i.e., junction cells convert a low current of high energy betas to a much larger current of low voltage electrons.

The efficiency of the P-N junction in converting the incident β radiation is very low. If silicon is used as the semiconductor, the major factor in reducing the efficiency arises from the fact that it takes approximately 4 ev to create an electron-hole pair whereas the maximum energy available for power output when the electron crosses the junction is 1.1 ev,

(the energy gap of silicon), thereby reducing the efficiency by nearly 73%. Other major factors reducing the efficiency, which will be explained later, are the voltage factor and the curve factor which reduce the efficiency to approximately 5%.

Power supplies based on the electron-voltaic effect have been described in the literature[1-4]. The measured radiation damage threshold of silicon has been found to be 200 kev[5,6]. Early cells used the radioisotope Sr^{90} which emitted betas up to 2 mev causing the power output of the cell to decrease rapidly due to radiation damage of the semiconductor. For this reason promethium^{147} (Pm^{147}) whose properties are listed in Table I has been accepted as the radioisotope in cell fabrication[4]. The maximum energy of the emitted betas is only 233 kev which exceeds the damage threshold of silicon but since the number of electrons having energy above this value is small, see Figure I-1, the degradation in power output caused by radiation damage appears negligible or at least tolerable.

P-N junctions used as energy converters of the betas emitted from Pm^{147} are generally made by diffusing phosphorus into 1 Ω cm boron-doped substrates at 875 - 975°C yielding minority carrier lifetimes between 1 and 10 μ sec[4]. It has been shown that large area epitaxial diodes can be grown that are superior, in terms of higher breakdown voltages which occur at lower reverse saturation currents, than large area shallow junctions fabricated by the diffusion technique[7]. Therefore, an investigation of the direct energy conversion of the betas emitted from the radioisotope Pm^{147} by silicon P-N junctions grown epitaxially by the chemical vapour deposition process was initiated. In addition the epitaxial growth process lends itself to controlled doping so that devices

TABLE I

Properties of Pm^{147}

$E_{B_{max}}$	230×10^3 ev	the maximum energy of beta particles
$E_{B_{av}}$	73×10^3 ev	average energy of beta particles
t_H	2.6 years	half-life
G	980 curies/gm	specific activity
I_{max}	1.1×10^{-3} amp/cm^2	self-absorption limited electron current which would be emitted from the surface of a semi-infinite layer
$2E_{B_{av}} I_{max}$	1.7×10^{-3} watts/cm^2	maximum power emitted from both faces of a thick planar source
α_o	1300 cm^{-1}	self-absorpiton coefficient of Pm^{147} beta rays
α_{Si}	380 cm^{-1}	Si absorption coefficient of Pm^{147} beta rays
α/ρ	150 cm^2/gm	mass absorption coefficient of Pm^{147} beta rays

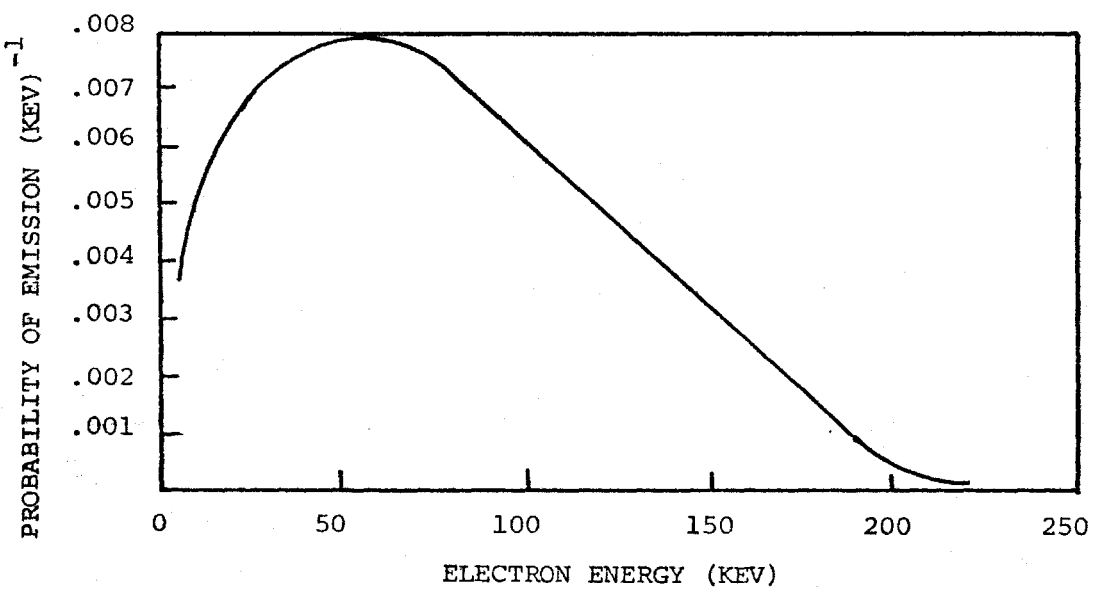

Figure I-1 Pm^{147} beta spectrum[3].

with several active junctions in series may be fabricated in one operation with no additional sample handling from growing a single junction device that might reduce device yield. The results obtained for the growth of the epitaxial P-N junctions and their energy conversion properties are presented in this thesis.

Previous investigations for the direct energy conversion of betas emitted from Pm^{147} using diffused $N^{+}P$ junctions have yielded short circuit currents (I_{sc}) of 20 μamp, open circuit voltage (V_{oc}) of 0.37 volts and maximum power outputs (P_m) of 5.2 μ watts and an efficiency of 1.85% for a source strength of 2 mg/cm^2 (8). The diodes fabricated in the present investigation were evaluated on a 2 mg/cm^2 Pm^{147} source. For a single junction device I_{sc} = 29 μ amp, V_{oc} = 0.37 volts and P_m = 7.2 μ watts; a double junction device yields I_{sc} = 15.2 μ amp, V_{oc} = 0.76 volts and P_m = 8 μ watts. The efficiency of these devices is approximately 3%.

CHAPTER II

P-N JUNCTION THEORY

2.1 Introduction

In this chapter a conventional description of the P-N junction found in most textbooks is repeated for completeness. The P-N junction is first examined in the unbiased state and then the current-voltage relationships are obtained when the junction is biased.

2.2 Some Aspects of P-N Junction Theory

Consider a single crystal semiconductor that contains one region of n-type material (electrons are the majority carriers) and one region of p-type material (holes are the majority carriers) thus forming a P-N junction. The initial boundary between the n-type material and the p-type material is known as the metallurgical junction. Due to the concentration gradients at the metallurgical interface the mobile electrons and holes diffuse into the p- and n-type regions respectively leaving behind ionized donors and acceptors. The ionized donors have a positive charge and the ionized acceptors a negative thereby causing a dipole field which counteracts the diffusive flow of electrons and holes. A condition of

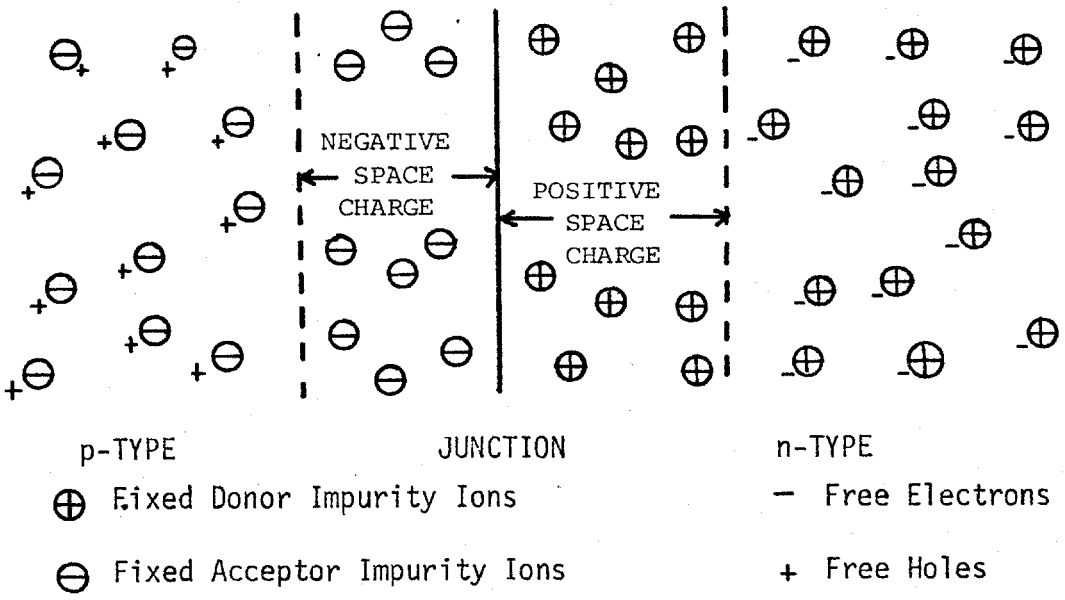

Figure 2-1 Illustration of the formation of space charge layers by diffusion of majority carriers near a junction to the region of opposite conductivity type.

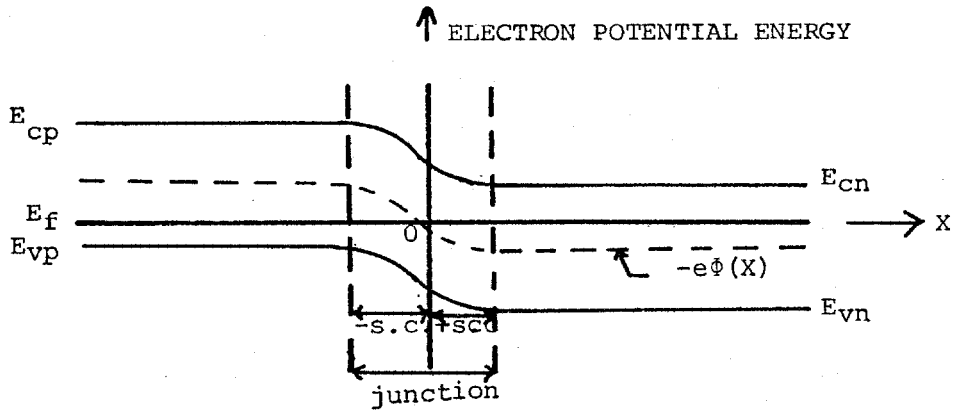

Figure 2-2 Potential energy diagram showing energy band configuration near a P-N junction in the presence of an applied bias.

dynamic equilibrium is reached whereby the regions adjacent to the metallurgical junction are depleted of majority carriers and in which exist strong space charge layers containing high electric fields. This condition is illustrated in Figure 2-1.

It is a well-known result of electrostatics that there is a difference in potential between the two extreme limits of an electric dipole layer which is related to the strength (dipole moment per unit area) of the layer by[9]:

$$\phi_2 - \phi_1 = 4\pi\Delta \qquad (2\text{-}1)$$

where ϕ_1 and ϕ_2 are the edge potentials and Δ is the dipole layer strength. Beyond the space charge regions there is no net charge density and therefore the electrostatic potential is constant. According to equation (2-1) the potential energy of an electron "at rest" at the bottom of the conduction band is lower by $4\pi e\Delta$ on one side of the junction than on the other. Similarly for holes "at rest" in the valance band. Since the state of the system is one of thermal equilibrium, however, the fermi energy, E_f, must be the same throughout the system. These conditions enable one to depict the energy bands of the semiconductor in the neighborhood of an abrupt junction as shown in Figure 2-2. There is clearly an "internal contact potential" built up between the two regions. The value of this contact potential is given by[9]:

$$\phi = \frac{kT}{e} \ln \frac{n_{n_o}}{n_{p_o}} = \frac{kT}{e} \ln \frac{p_{p_o}}{p_{n_o}}$$

where n_{n_o} (p_{p_o}) is the electron (hole) concentration in the n- (p-) type region under thermal equilibrium and n_{p_o} (p_{n_o}) is the electron (hole) concentration in the p- (n-) type region under thermal equilibrium. This may be written as:

$$\phi = \frac{kT}{e} \ln \frac{N_a N_d}{n_i^2} \qquad (2\text{-}2)$$

when all the donors (N_d) and acceptors (N_a) are ionized; n_i is the intrinsic carrier concentration of the semiconductor at temperature T. From equation (2-2) it is apparent that the contact potential is greater the larger the doping of the n and p sides of the junction.

Some other aspects of the space charge region and the electric field are:

(a) The space charge layer is of greater extent in lightly doped p- or n-type regions than in regions which are heavily doped. For a given junction the space charge layer extends furthest into the region which is least heavily doped. That is for an N^+P junction the space charge region exists almost entirely within the p-type region where N^+ designates a heavily doped semiconductor.

(b) The maximum field value is very high in heavily doped junctions and smaller in junctions where one or both sides are lightly doped.

(c) Under reverse bias conditions the space charge regions extend out into the crystal while under forward bias they are compressed.

In the equilibrium state of a P-N junction there will be a certain number of electrons in the n-type region with sufficient energy to surmount the potential barrier and diffuse into the p-type side. These electrons have now changed from majority carriers to minority carriers. In the p-type region these minority carriers will then recombine with holes after a finite time. Therefore, in equilibrium, we have a "recombination" current, J_{nr}, set up whereby electrons diffuse from the n-type region into the p-type region where they recombine with holes. However, in the equilibrium condition there is no net current flow; furthermore, according to the principle of detailed balance, at equilibrium any microscopic transport process and its inverse must proceed at equal rates. In this case the reverse process is the thermal generation of electrons in the p-type region which easily diffuse down the potential barrier into the n-type region where they become majority carriers creating a generation current, J_{ng}. At equilibrium $J_{ng} = - J_{nr}$. Similarly for holes we have $J_{pg} = -J_{pr}$. That is the total fluxes of holes and electrons across the junction under equilibrium conditions is equal to zero.

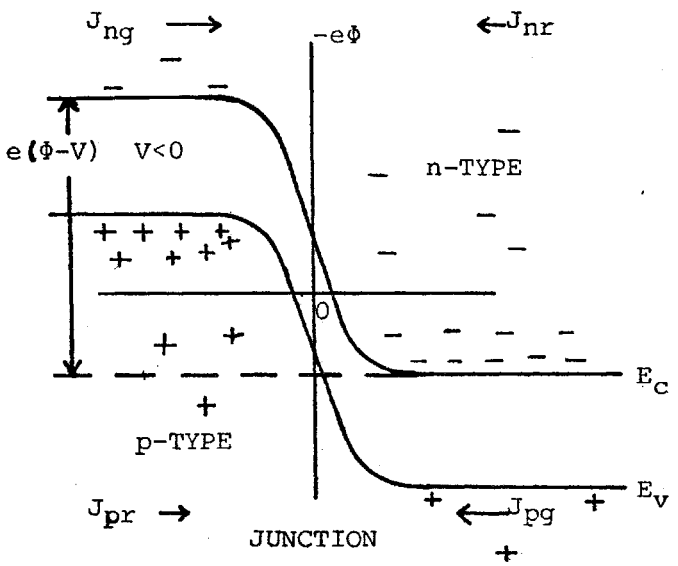

(a)

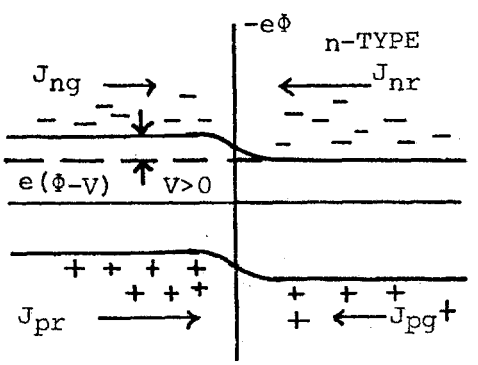

(b)

Figure 2-3 Potential diagram of a P-N junction (a) with reverse bias, (b) with forward bias, showing how generation and recombination fluxes are modified.

Let us now examine the P-N junction under non-equilibrium conditions as in the case when a bias is applied. From Figure 2-3(a) when a reverse bias is applied the potential barrier is increased to $e(\phi-V)$ and the currents J_{nr} and J_{pr} are substantially reduced due to the fact that the majority carriers now find it more difficult to surmount the potential barrier. The fluxes J_{ng} and J_{pg}, however, depend only on the thermal generation of electron-hole pairs and are unaffected by the applied bias. As the bias is increased the current density across the junction approaches a constant value - $e(J_{pg}-J_{ng})$ called the saturation current which is limited to the thermal generation of electron-hole pairs in the bulk regions near the depletion region. This current depends solely on material parameters and temperature and is independent of the applied voltage. It must be noted, however, that after a certain voltage is applied certain phenomena exist which drastically increase the current. This voltage is known as the breakdown voltage.

With the application of a forward bias as in Figure 2-3(b) the potential barrier is reduced and it now becomes easier for the diffusion of majority carriers across the junction thus increasing J_{nr} and J_{pr} above their equilibrium values. The generation currents, J_{ng} and J_{pg}, remain constant but the overall effect is that large currents may arise. Thus we have a low impedance device in the forward bias condition and a high impedance device in the reverse bias state.

By solving the continuity equation for excess minority carriers in both the p- and n-type regions and applying the appropriate boundary conditions one is able to obtain the current-voltage characteristics of

the junction. It will be assumed that a steady state has been reached and that all voltage drops occur only in the space charge regions. The continuity equations are[9]:

$$D_p \frac{\partial^2 \Delta p}{\partial x^2} - \frac{\Delta p}{\tau_p} = 0 \text{ for the n-type region}$$

$$D_n \frac{\partial^2 \Delta n}{\partial x^2} - \frac{\Delta n}{\tau_p} = 0 \text{ for the p-type region}$$

where $\Delta n(\Delta p)$ is the excess electron (hole) concentration

$D_n(D_p)$ is the electron (hole) diffusion coefficient

$\tau_n(\tau_p)$ is the electron (hole) minority carrier lifetime

These are subject to the boundary conditions:

$$\frac{n_p}{n_{p_0}} = \frac{p_n}{p_{n_0}} = \exp\left(\frac{eV}{kT}\right)$$

at the junction where n_{p_0} is the equilibrium electron concentration in the p-type region

$$\Delta n_p = n_p - n_{p_0}$$

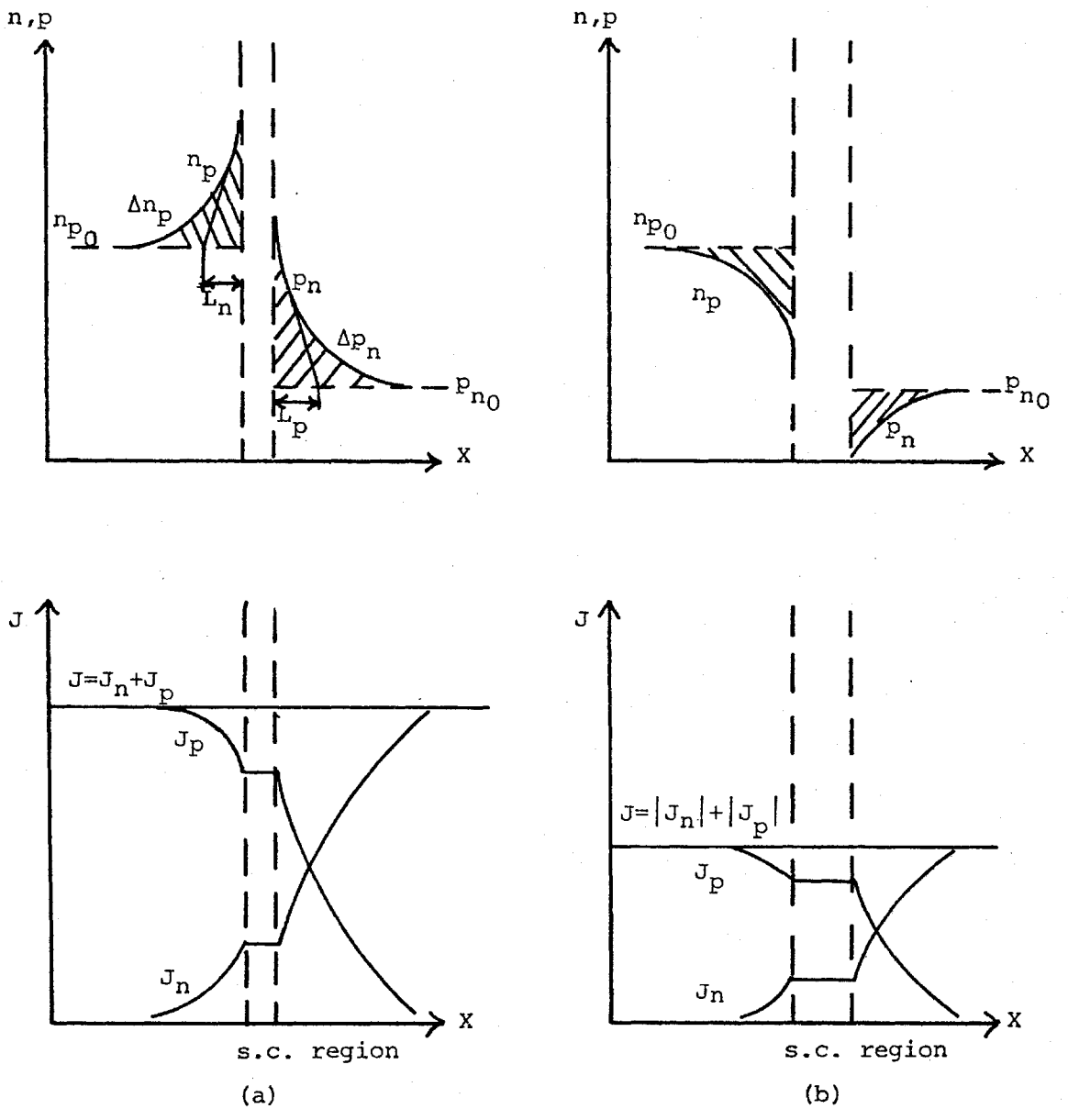

Figure 2-4 Electron and hole concentrations and fluxes in the neighbourhood of a P-N junction (a) with forward bias, (b) with reverse bias.

similarly for p_n, p_{n_0} and Δp_n and

$$\Delta n_p = \Delta p_n = 0$$

far from the junction.

Using this procedure one first calculates the excess carrier concentrations which are shown in Figure 2-4[10] and from these are determined the electron and hole currents. By assuming that there is no generation or recombination in the space charge region we arrive at the diffusion controlled ideal diode equation sometimes called the Shockley equation[10]:

$$I = en_i^2 \left(\frac{D_n}{p_{p_o} L_n} + \frac{D_p}{n_{n_o} L_p} \right) (\exp (eV/kT) - 1) \qquad (2\text{-}3)$$

where $J_{ng} = \frac{D_n}{p_{p_o} L_n}$ and $J_{pg} = \frac{D_p}{n_{n_o} L_p}$

and D_n and D_p are the minority carrier diffusion coefficients for electrons and holes respectively,

and L_n and L_p are the minority carrier diffusion lengths for electrons and holes respectively,

$L = \sqrt{D\tau}$ where τ is the minority carrier lifetime. The reverse saturation current I_o is given by $I_o = e(J_{ng} + J_{pg})$.

Although this equation adequately describes germanium P-N junctions at low current densities, it is only qualitative for other materials. The departures from ideal behaviour are due mainly to the following effects:

(1) the surface leakage effect

(2) generation-recombination in the depletion region

(3) tunneling of carriers in the band gap

(4) the high injection condition, which may occur at relatively small forward bias

(5) the series resistance effect.

For silicon planar junctions we need not consider the surface leakage current because in general it is much smaller than the generation-recombination current in the depletion region. The effect of the generation-recombination current in the depletion region is to increase I_o and to add to the forward current at low biasing. Experimentally the forward current has the following empirical form[10]:

$$I = I_o \left(\exp\left(\frac{eV}{nkT}\right) - 1\right) \qquad (2\text{-}4)$$

where n = 2 when the generation-recombination current dominates and n = 1 when the diffusion current dominates. In general for silicon diodes n = 2 for small applied voltages and n = 1 for higher voltages where the diode current is diffusion controlled. The effects of high injection and series resistance is to reduce the slope of the forward curve.

CHAPTER III

THE P-N JUNCTION AS AN ENERGY CONVERTER

3.1 Introduction

This chapter describes the effect of irradiating a P-N junction with a beam of β-particles. It is shown that the P-N junction when irradiated can be used to supply power to a load. Several of the material parameters which influence the power output of the irradiated junction are also discussed.

3.2 The P-N Junction as an Energy Converter

Radioactivity can be converted to useful electrical power by means of a P-N junction. Electron-hole pairs produced in the semiconductor by beta radiation or light, for example, are separated by the junction field; the separated pairs bias the junction in the forward direction and deliver power to a load. For optical radiation -- sunlight, for example -- each photon with energy equal to or larger than the band gap of the semiconductor produces one electron-hole pair. The energy in each photon in excess of the band gap is absorbed as phonon energy. For beta particles,

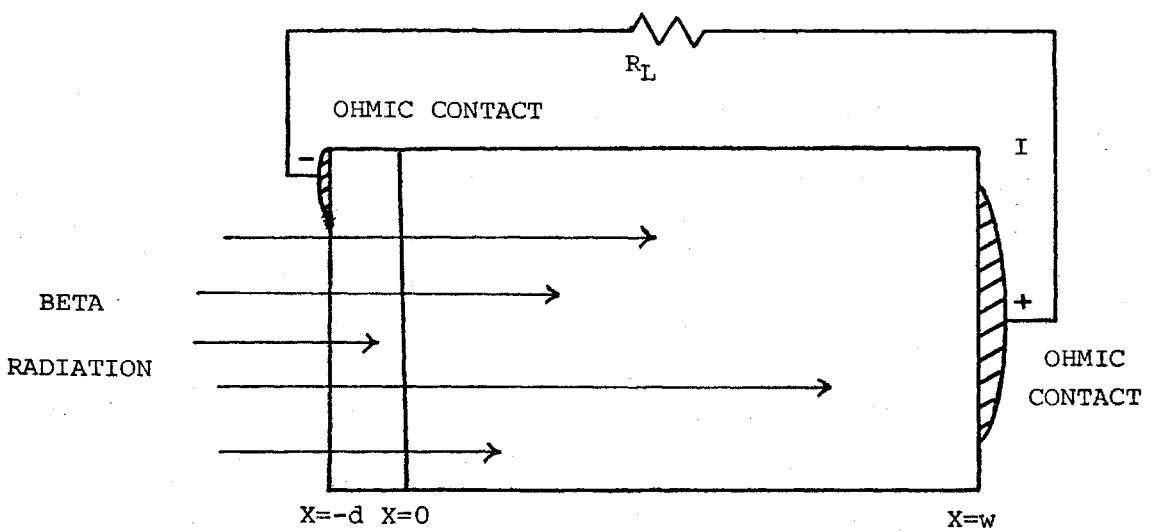

Figure 3-1 Geometry of a diode used as a beta-voltaic energy converter.

however, each beta may produce many electron-hole pairs until its energy is less than that required for the generation of one electron-hole pair. The beta particles are absorbed exponentially with distance of penetration and have the absorption coefficient given in Table I. The average energy, w (in electron volts) expended in the generation of one electron-hole pair is given by w = Eg + 2.5 (or 3.6 ev for silicon) as indicated by the data of McKay and McAfee[11]. Bussoloti et al[12] have reported a value of w = 3.8 while Vavilov[13] reported w = 4.2. Both these measurements were determined from electron bombardment measurements. The combination of a P-N junction with a beta-emitting radioisotope may be looked upon as a dc transformer, since the low current and high voltage of the electrons emitted by the radioisotope are transformed into a high current at a low voltage.

In order to evaluate material parameters in the construction of P-N junctions employing the electron-voltaic effect for energy conversion using a beta-emitting radioisotope it is necessary to understand the processes involved when the junction is irradiated by betas emitted from the radioisotope. An irradiated junction is shown in Figure 3-1. First consider the case when the P-N junction is connected to an open circuit. Excess electrons are created in the p region and excess holes in the n region. It must be noted that for each excess minority carrier generated in a given region there is also an excess majority carrier generated but this excess creates a negligible increase in majority carrier concentration whereas the minority carrier concentration changes by orders of magnitude.

Excess electrons in the p region may diffuse to the junction and descend the potential barrier into the n region while the excess holes in the n region may diffuse to the junction and float up the potential barrier into the p side thus reducing their energy. When this occurs an excess positive charge is created on the p side of the junction and an excess negative charge on the n side. This effectively forward biases the junction so that the barrier height is reduced by an amount V_{oc} to some value $\phi - V_{oc}$. This counteracts the flow of current in the junction which would otherwise occur. The internal voltage is now different from the contacting potentials at the device terminals and a voltage equal to the difference, V_{oc}, will appear at the circuit terminals. This phenomenon is known as the electron voltaic effect. The magnitude of this voltage may be determined by the carrier concentrations at the edge of the space charge regions[9].

$$\frac{p_n}{p_{n_o}} = \frac{n_p}{n_{p_o}} = \exp\left(\frac{eV_{oc}}{kT}\right) \qquad (3\text{-}1)$$

where p_n and n_p are the minority hole and electron concentrations due to irradiation. In the open circuit condition of the irradiated junction the generation currents, J_{ng} and J_{pg}, are increased while the recombination currents, J_{nr} and J_{pr}, are initially unaltered. The resulting unbalanced diffusion currents cause a net charge accumulation whose field lowers the initial barrier height, thus enabling the recombination currents to increase until a balance between generation and recombination is once more achieved, giving rise to a voltage across the device terminals. If we now

short out the device terminals an electric current will flow therein as long as there is a diffusion current of irradiation created excess minority carriers into regions where they become majority carriers in order to maintain the internal barrier height at ϕ. In this condition the generation currents are always larger than the recombination currents (which have no inherent dependence on the radiation intensity) except through damage creation. It is these generation currents continuing as long as the device is irradiated which provide the source of current which flows in the external circuit.

To determine the current-voltage characteristics of the irradiated junction the continuity equations for the minority carriers must be examined as in the development of the Shockley diode equation. Moreover, the generation of carriers due to the radiation must be added. The continuity equations for an infinitely planar junction become:

$$g - \frac{\Delta p}{\tau_p} - \frac{\partial Jp}{\partial x} = \frac{\partial \Delta p}{\partial t} \quad \text{for the n-type region} \qquad (3\text{-}2a)$$

and

$$g - \frac{\Delta n}{\tau_n} - \frac{\partial Jn}{\partial x} = \frac{\partial \Delta n}{\partial t} \quad \text{for the p-type region} \qquad (3\text{-}2b)$$

where Δn and Δp are the excess minority carrier concentrations above their equilibrium values and g is the generation rate of carriers caused by the radiation impinging on the surface of the device. Assume g takes the form $g = \alpha N e^{-\alpha x}$ [14] where α is the absorption coefficient of the semiconductor and N is the incident electron flux.

Assuming that no electric fields exist outside the space charge region the continuity equations for the steady state become:

$$\alpha N e^{-\alpha x} - \frac{\Delta p}{\tau_p} + D_p \frac{\partial^2 \Delta p}{\partial x^2} = 0 \qquad (3\text{-}3a)$$

and

$$\alpha N e^{-\alpha x} - \frac{\Delta n}{\tau_n} + D_n \frac{\partial^2 \Delta p}{\partial x^2} = 0 \qquad (3\text{-}3b)$$

let $x = 0$ at the junction which is at a depth d below the surface which is irradiated. The general solutions to these equations are well known.[9]

for $x > 0$

$$\Delta n = A \exp\left(\frac{x}{L_n}\right) + B \exp\left(-\frac{x}{L_n}\right) + \frac{\alpha N \tau_n}{1-\alpha^2 L_n^2} \exp - \alpha(x+d) \qquad (3\text{-}4a)$$

for $x < 0$

$$\Delta p = C \exp\left(\frac{x}{L_p}\right) + D \exp\left(-\frac{x}{L_p}\right) + \frac{\alpha N \tau_p}{1-\alpha^2 L_p^2} \exp - \alpha(x+d) \qquad (3\text{-}4b)$$

Consider a device with $d >> L_p$, that is one in which the p and n regions are both infinite in the x direction. Thus we have a condition in which Δn and Δp must decay to zero at large values of x and therefore the arbitrary constants A and C must be zero. We may determine B and D by using the boundary conditions at the junction:

$$\frac{n_p(o)}{n_{p_o}} = \frac{p_n(o)}{p_{n_o}} = \exp\left(\frac{ev}{kT}\right) \tag{3-5}$$

Note that $n_p(o) = n_{p_o} + \Delta n(o)$ and $p_n(o) = p_{n_o} + \Delta p(o)$.

$$B = p_{n_o} \exp\left(\frac{ev}{kT} - 1\right) - \frac{\alpha N \tau_p}{1-\alpha^2 L_p} \exp(-\alpha d) \tag{3-6a}$$

$$D = n_{n_o} \exp\left(\frac{ev}{kT} - 1\right) - \frac{\alpha N \tau_n}{1-\alpha^2 L_n^2} \exp(-\alpha d) \tag{3-6b}$$

Knowing the excess carrier concentrations the current densities into the P-N junction may now be determined by evaluating the diffusion currents on both sides of the junction.

$$J_n(o) = D_n \left(\frac{\partial \Delta n}{\partial x}\right)_{x=0} \quad \text{and} \quad J_p(o) = D_p \left(\frac{\partial \Delta p}{\partial x}\right)_{x=0}$$

$$I = e\,(J_p(o) - J_n(o))$$

$$= e\left(\frac{p_{n_o} D_p}{L_p} + \frac{n_{p_o} D_n}{L_n}\right) \exp\left(\frac{eV}{dT} - 1\right) - \frac{e\alpha N L_p}{1-\alpha^2 L_p^2} (1-\alpha L_p) \exp(-\alpha d) \tag{3-7}$$

$$- \frac{e\alpha N L_n}{1-\alpha^2 L_n^2} (1-\alpha L_n) \exp(-\alpha d)$$

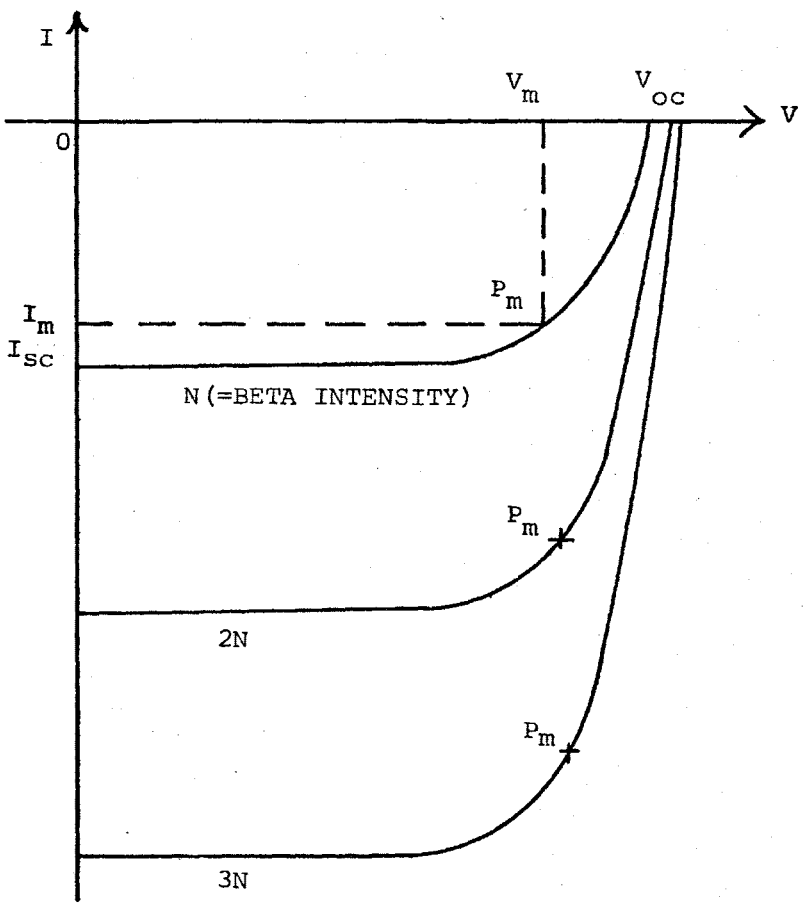

Figure 3-2 Current-voltage relation for a P-N junction beta-voltaic device under different radiation intensities, showing the maximum power points.

This may be expressed as:

$$I = I_o \left(\exp\left(\frac{eV}{kT}\right) - 1\right) - I_g \qquad (3\text{-}8)$$

where the first term is the Shockley diode equation and the second is the generation current caused by the betas irradiated into the junction. It can be shown that no matter what the values of α, L, and d are, I_g is always positive[10] so that for the irradiated junction the initial forward portion of the I-V curve is in the fourth quadrant. The current voltage relationships for the irradiated diode are illustrated in Figure 3-2 for several different intensities of the beta flux.

If the circuit resistance (including the internal resistance of the device itself) approaches zero, then the voltage is negligibly small and we have the short circuit condition corresponding to a current density of the diode:

$$I_{sc} = -I_g \qquad (3\text{-}9)$$

When the current is zero (i.e., we have an infinite load across the device terminals) we have the open circuit condition such that:

$$V_{oc} = \frac{kT}{e} \ln\left(\frac{I_g}{I_o} + 1\right) \qquad (3\text{-}10)$$

As indicated from equations (3-7) and (3-8) the generation current is proportional to the intensity of the irradiation whereas the

open circuit voltage varies logarithmically through I_g of equation (3-10). This leads to the family of curves shown in Figure 3-2.

The maximum power which may be obtained from the junction for a given radiation intensity may be found by the area of the largest rectangle which may be inscribed in the fourth quadrant of the I-V curve. From equation (3-10) it is evident that V_{oc} increases as I_{sc} increases and I_o decreases. The reverse saturation current, I_o, may be written as:[10]

$$I_o = en_i^2 \left(\frac{1}{N_A} \left(\frac{D_p}{\tau_p} \right)^{1/2} + \frac{1}{N_D} \left(\frac{D_n}{\tau_n} \right)^{1/2} \right) \qquad (3\text{-}11)$$

if all the acceptors (N_A) and donors (N_D) are ionized. From this expression the condition that I_o be low implies that the minority carrier lifetimes be large as well as the dopant concentrations in the n- and p-type regions. The maximum open circuit voltage available is equal to the internal potential barrier of the junction which, from equation (2-2), is a function of doping densities increasing as N_A and N_D increase. However, it is found that for high impurity concentrations the minority carrier lifetime decreases. Thus to obtain low saturation currents we must find the optimum conditions for doping densities and minority carrier lifetimes.

It is necessary to obtain large generation currents for high power outputs for two reasons:

(1) an increase in I_g increases the open circuit voltage according to equation (3-10)

(2) the larger I_g the larger is the current available for the power output ($p_m = I_m V_m$).

From equation (3-7) we find that an increase in minority carrier lifetimes (and thus diffusion lengths) will lead to an increase in I_g. It should be also noted that minority carrier lifetimes have a larger effect on I_g than V_{oc} and it is mainly for this reason that highly doped materials are not used for both n- and p-type sides of the junction. However, if one constructs a junction so that it is one sided shallow abrupt junction with the base region being the lighter doped and having a long minority carrier lifetime most of the incident energy will be absorbed within the base and the minority carriers so generated can be collected at the junction. In such cases, we may make the top region of the device heavily doped but thin enough so that most minority carriers created in this layer are collected by the junction. In this way we are able to increase the built-in potential of the junction while tolerating a low minority carrier lifetime in one side of the junction.

Devices made with shallow junction depths, d, such that $d \sim L_p$ as for the diode illustrated in Figure 3-1, change the boundary conditions used in finding I_g in equation (3-7). In this case we must use a different boundary condition for the n-type layer. At $x = -d$:

$$D_n \left(\frac{d\Delta n}{dx} \right)_{x=-d} = S \cdot [n_p(-d) - n_{p_o}] \qquad (3\text{-}12)$$

where S is the surface recombination velocity. For the p-type region let us use a finite length w and at $x = w$, $\Delta n = 0$ (i.e., we have an ohmic contact). These conditions lead to a different expression for I_o such that larger values of S tend to increase the reverse saturation current.

More important however is the effect on the generation current which becomes[15]:

$$I_g = e\alpha N \frac{L_n \exp(-\alpha d)}{\alpha^2 L_n^2 - 1} (1 - \alpha^2 n) + \frac{\exp(-w/L_n) - \exp(-\alpha d)}{\sinh (w/L_n)} \qquad (3\text{-}13)$$

$$+ \frac{L_p}{\alpha^2 L_p^2} (1 - \alpha L_p) \exp(-\alpha d) + \frac{S + \alpha D_p - (D_p/L_p + S) \exp d (1/L_p - \alpha)}{S \sinh (d/L_p) + D_p/L_p \operatorname{dosh} (d/L_p)}$$

From this expression one finds that as w decreases below L_n, I_g decreases. It has also been shown that L_p has a deleterious effect when $L_p < 2d$. For solar cells the surface recombination velocity has a negligible effect on the generation current below 10^4 cm/sec and a maximum over the range $10^6 - 10^8$ cm/sec[15].

The material parameters affecting the maximum current and voltage outputs of an irradiated P-N junction have now been discussed. As has already been discussed the available power obtained from an irradiated P-N junction comes from the area of the power rectangle inscribed in the fourth quadrant of the I-V curve. The maximum power obtainable comes from the largest rectangle so inscribed which must have one of its corners in the knee of the curve. It is obvious that the maximum power given by $p_m = I_m . V_m$ does not equal the product of $I_{sc} . V_{oc}$. This could only occur if the curve were square rather than the exponential of the Shockley equation. It has already been pointed out that in reality the exponential has the form exp eV/nkT. The effect of values of n larger than 1 is to

make the curve even more rounded and thus reduce the available output power. In solar cells n has been found to have a value larger than 2 for voltages less than 0.4 volts and n = 1 for voltages larger than 0.5 volts[16].

Other effects which tend to reduce output powder by flattening the knee of the I-V curve are effects arising from series and shunt resistances. The series resistance includes the contact resistance -- those of the terminals and base region of the cell -- and the sheet resistance of the top layer. The series resistance effect is greater at high current levels than at lower ones and can have disastrous effects on the output performance of solar cells for values as small as 1 Ω[17]. The shunt resistance, R_{Sh}, adds a positive term, V/R_{Sh}, to the current of the ideal diode equation. This effect is observed at low biasing but if the shunt resistance is very low the effect is observed at higher voltages.

3.3 Multi-junction Cells for Energy Conversion

In this section is presented a simplified theoretical treatment of an irradiated multi-junction device which acts as two diodes in series. That is, the device when subjected to the betas emitted from the promethium ^{147} should yield an open circuit voltage which is double that of a single junction cell. The energy band diagrams of three possible structures for a two diode in series structure are shown in Figure 3-3. In order to have the two diodes in series it is necessary to have an ohmic

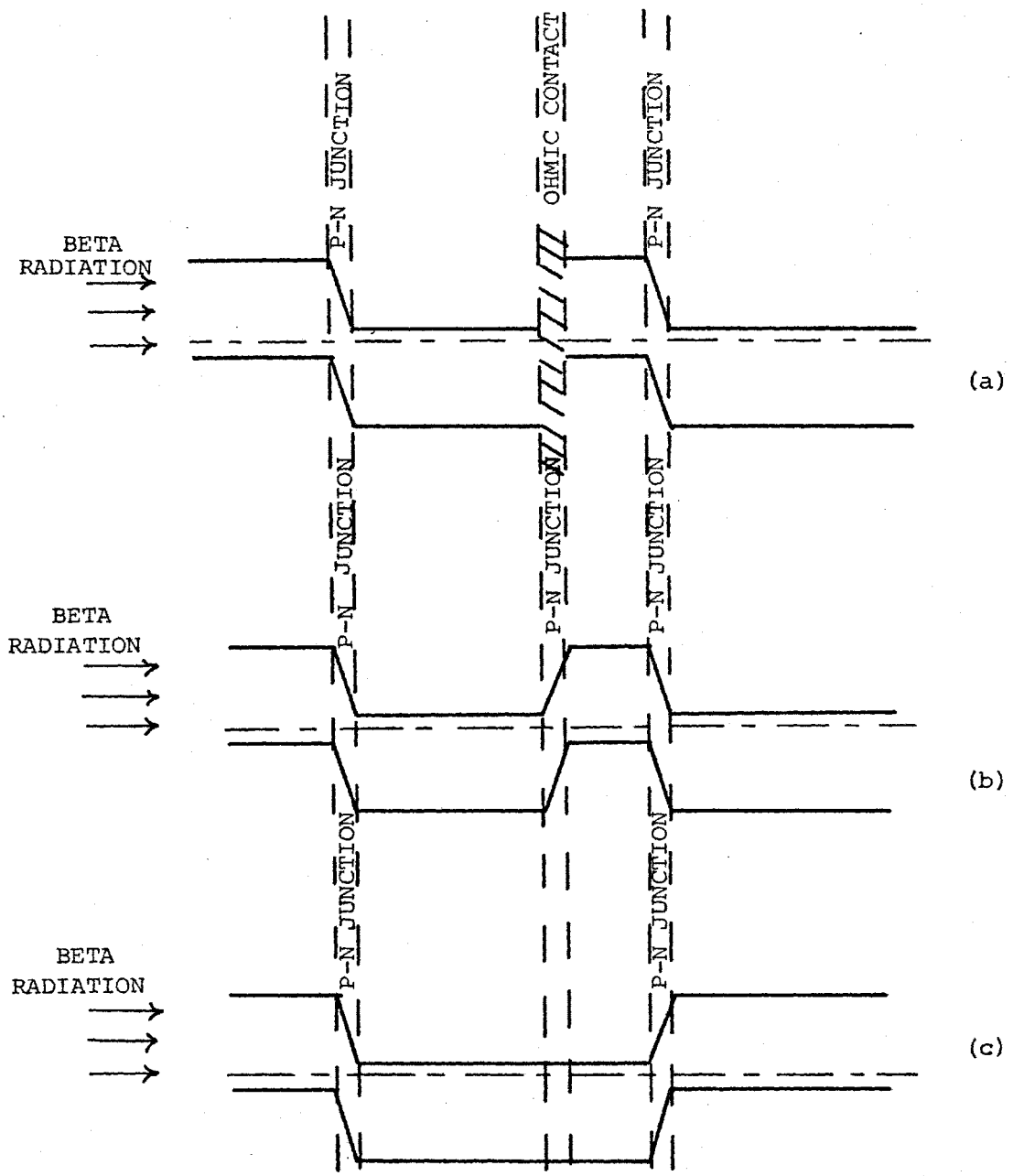

Figure 3-3 Energy band diagrams for the proposed structures for the construction of two diodes in series.

contact between the N^+ region of one diode and the p-region of the other as shown in Figure 3-3(a). If the two useful energy converting junctions were not separated in this manner the structure of the device would be that of Figure 3-3(b) or (c). In Figure 3-3(b) there are three junctions which can become forward biased when irradiated. The voltage developed across the middle junction, however, is opposite in sign to the two on the outside and would subtract from them resulting in a total voltage less than the sum of that derived from two junctions. In Figure 3-3(c) the two junctions when irradiated would develop voltages opposite in sign a and the effective output voltage of the device would approach zero.

A problem arises in obtaining the ohmic contact shown in Figure 3-3(a). Previously this had been achieved by growing the two diodes separately and matching metallization grids on the back of one diode and on the top of the second diode[14]. In the present investigation this was achieved by growing a P^+ layer between the N^+ and P regions in place of the ohmic contact shown in Figure 3-3(a). It is the resulting $N^+PP^+N^+P$ structure which will be described in this section.

When the $N^+PP^+N^+P$ structure shown in Figure 3-4 is irradiated by beta radiation it is the transport of minority carriers which determine the current-voltage characteristics of the device. The continuity equations for the minority carriers are:

$$g - \frac{p}{\tau_p} - \frac{\partial J_p}{\partial x} = \frac{\partial p}{\partial t} \qquad \text{for the N-regions}$$

$$g - \frac{n}{\tau_n} - \frac{\partial J_n}{\partial x} = \frac{\partial n}{\partial t} \qquad \text{for the P-regions}$$

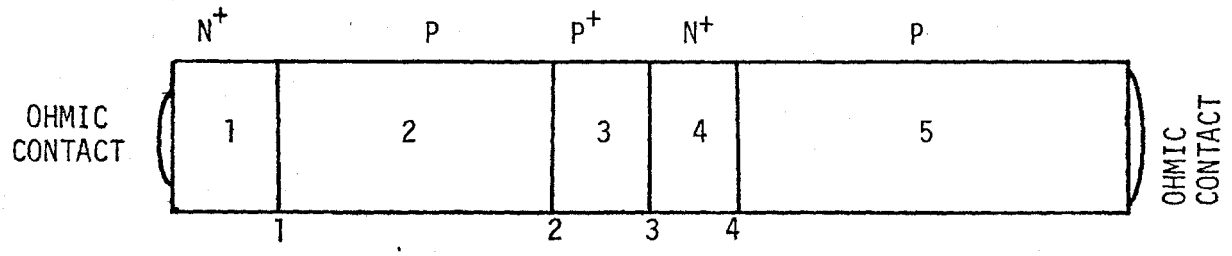

Figure 3-4 Structure of two diodes in series.

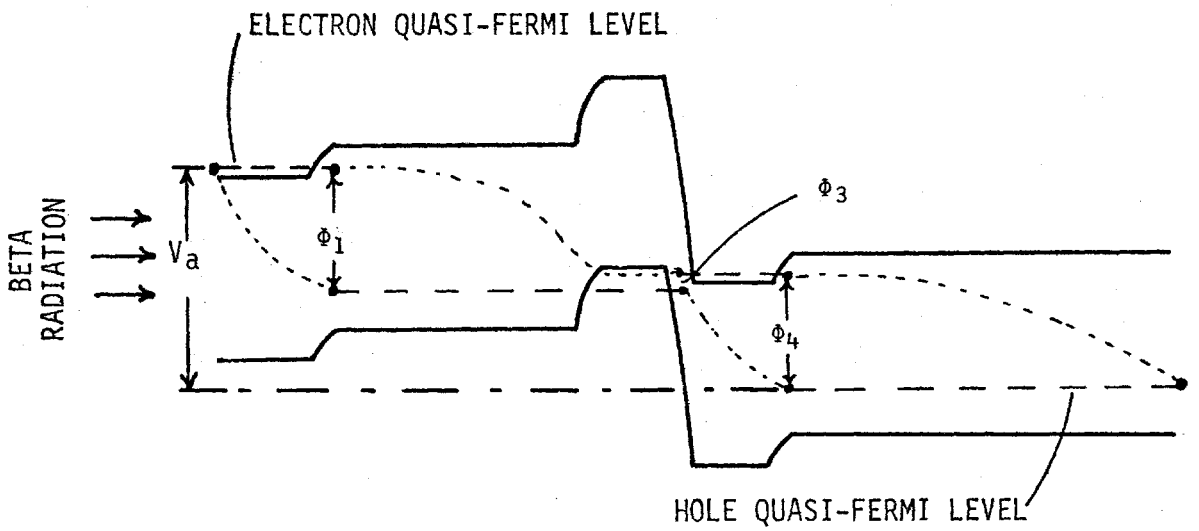

Figure 3-5 Energy band diagram for the $N^+PP^+N^+P$ structure of two diodes in series illustrating the quasi-fermi levels and junction potentials for an irradiated device.

If we assume there are no electric fields in the bulk of the semiconductor and that the generation rate is given by $g = \alpha N e^{-\alpha x}$ (16), then the continuity equations become:

$$\alpha N e^{-\alpha x} - \frac{p}{\tau_p} + D_p \frac{\partial^2 p}{\partial x^2} = \frac{\partial p}{\partial t}$$

and

$$\alpha N e^{-\alpha x} - \frac{n}{\tau_n} + D_n \frac{\partial^2 n}{\partial x^2} = \frac{\partial n}{\partial t}$$

Assuming that a steady state has been reached (i.e., $\partial p/\partial t = \partial n/\partial t = 0$) solutions to the continuity equations are:

in the p-regions:

$$\Delta n = A_i e^{x/L_n} + B_i e^{-x/L_n} - \frac{N e^{-\alpha/L_n}}{L_n D_n (1 - 1/L_n^2 \alpha^2)}$$

and in the N-regions:

$$\Delta p = C_i e^{x/L_p} + D_i e^{-x/L_p} - \frac{N e^{-\alpha/L_p}}{L_p D_p (1 - 1/\alpha^2 L_p^2)}$$

Knowing the excess minority carrier concentrations we may determine the electron and hole current flows:

$$J_n = q D_n \frac{\partial n}{\partial x} = q D_n \frac{\partial \Delta n}{\partial x}$$

and

$$J_p = - q D_p \frac{\partial p}{\partial x} = q D_p \frac{\partial \Delta p}{\partial x}$$

Therefore in the P regions we have:

$$J_{n/q} = \frac{D_n A_i}{L_n} e^{x/L_n} - \frac{D_n B_i}{L_n} e^{-x/L_n} + \frac{N e^{-\alpha x}}{(1-1/\alpha^2 L_n^2)}$$

and in the N regions:

$$J_{p/q} = - \frac{D_p C_i}{L_p} e^{x/L_p} + \frac{D_p C_i}{L_p} e^{-x/L_p} - \frac{N e^{-\alpha x}}{(1-1/\alpha^2 L_p^2)}$$

Thus we have ten unknowns -- A_2, B_2; A_3, B_3; A_5, B_5 for the P regions and C_1, D_1; C_4, D_4 for the N regions -- which must be solved. This is done by matching at the junctions.

Assume:

(1) The quasi-fermi levels are constant across the junction. That is at junction 1 for example $p_1 N_D = n_i^2 e^{q\phi/kT} = n_i N_A$ where ϕ is the difference between the electron and hole quasi-fermi levels and is not the contact potential described earlier.

(2) The front and back contacts are ohmic. That is $p_f N_D = n_i^2 = n_b N_A$.

These two assumptions give six equations for the A, B, C, D - four from the junctions and two from the contacts.

(3) Assume the generation and recombination in the junctions are negligible.

$$J_{n_i} + J_{p_i} = J_{diode} = \text{constant}$$

Also $$J_{p_2} = J_{p}{}_{2}^{+}$$

This implies 3 more equations which give three additional relationships for the A, B, C, D.

Let junction 3 be a tunnelling junction such that:

$$J_{n_3} + J_{p_4} + J_{tun} = J_{diode}$$

It should be noted that J_{tun} is a function of ϕ_3.

Thus far there are nine equations for the ten unknowns and one more equation is necessary to solve for the unknowns. This is shown from the fermi level shifts of the irradiated diode shown in Figure 3-5. Assuming changes in the majority carrier quasi-fermi levels are negligible:

$$V_a = \phi_1 - \phi_3 + \phi_4 = V_{oc}$$

Using this last relationship adds the tenth equation. The technique used to solve for the unknowns was to specify ϕ_3 which then allowed J_{tun} to be calculated. The ten equations were set up and solved simultaneously by Gaussian reduction. This allows J_{diode} and V_a to be calculated for each N, α, junction depth and doping density. If tunnelling is easy, i.e., ϕ_3 approaches zero, the problem is identical to treating two distinct diodes in series. That is the current for the overall diode may be expressed as $I = I_o$ (exp qV/nkT - 1) where $V = V_1 + V_2$ and $n = n_1 + n_2$; or for two identical diodes $V = 2V_1$ and $n = 2n_1$. This means that the open circuit voltage of the double diode will be twice that of the single diode structure. However, if junction 3 does not tunnel then no increase in V_{oc} over a single diode is observed in the numerical calculations. It was also found the layers 2 and 3 possess optimum values for obtaining the maximum power output. The optimum thickness (see Appendix E) for the layers are:

N_1^+ = 1.0 microns

P_2 = 13 microns

P_3^+ = 1.5 microns

N_4^+ = 1 micron

P_5 = 250 microns (substrate thickness)

3.4 Efficiency of the P-N Junction as a Beta Energy Converter

In this section the term efficiency refers to the ability of a device to convert the energy of the beta input flux into electrical energy. That is what fraction of the incident power can be converted into electrical power.

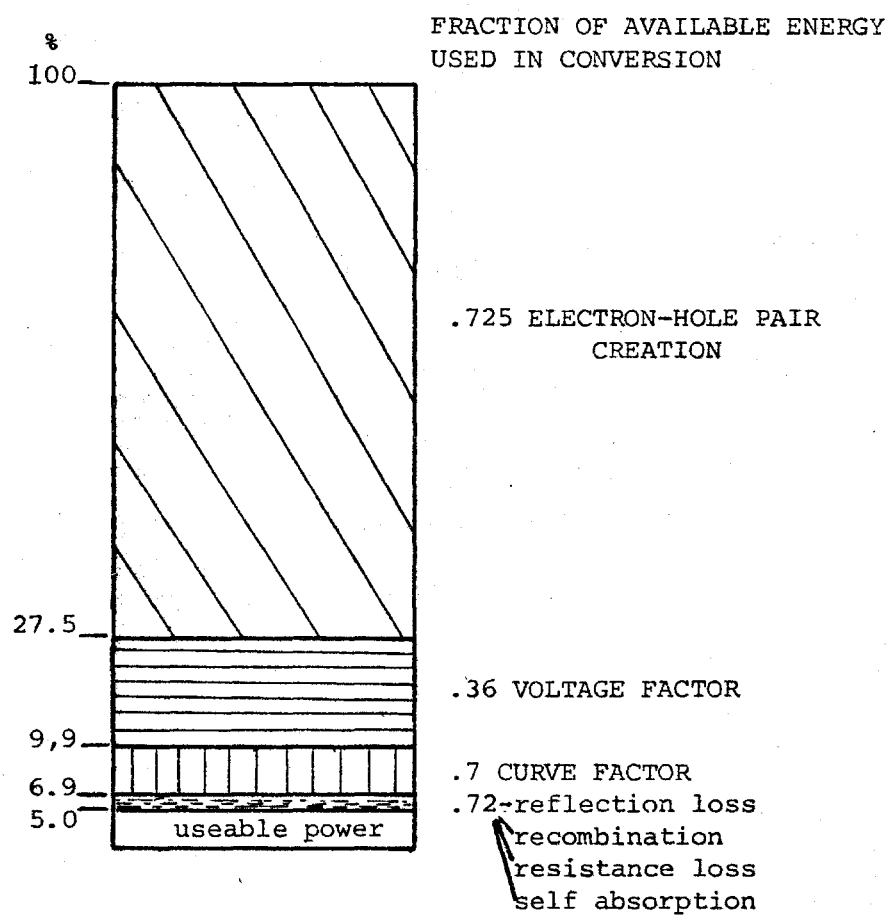

Figure 3-6 Block diagram showing energy losses which reduce the efficiency of a P-N junction as a beta-voltaic energy converter.

Figure 3-6 is a block diagram representing the power losses which reduce the efficiency of the P-N junction as a beta-voltaic energy converter. The power losses are due to three main factors: (1) the high energy needed to create an electron hole pair, (2) the voltage factor, (3) the curve factor. Factor (1) represents 72.5% of the power losses. This factor is so large because for electron bombardment it takes 4 ev[12,13] to create an electron-hole pair rather than the 1.1 ev of the energy gap for silicon. That is the maximum energy available when the electrons or holes diffuse to the junction is 1.1 ev when the minority carriers cross the junction. Therefore, the maximum amount of energy available from any one of the minority carriers is 1.1 ev whereas it takes 4 ev to create it.

The 4 ev needed for electron-hole pair generation by beta particles is much larger than the 1.1 ev necessary for photon generated electron-hole pairs. However, Shockley has shown[38] that the energy for electron-hole pair generation by beta particles may be written as:

$$W = E_g + E_{ph} + E_f$$

where E_g is the energy gap

E_{ph} is the energy of the incident particle that is converted into phonon energy before the actual ionization occurs

E_f is the final energy of the electron or hole which is very quickly (10^{-12} sec) dissipated as phonon energy.

Thus the extra energy needed in creating the electron hole pair is absorbed as phonon energy. It should be noted that for the energies of the beta

particles emitted by the promethium^{147} almost all is used for ionization, i.e., the formation of electron-hole pairs, and hardly any for atomic collision(18).

Factor (2), the voltage factor, is the ratio by which the open circuit voltage is smaller than the energy gap and is given by V_{oc}/E_g. This accounts for the fact that not all the energy of the energy gap (1.1 ev) can be obtained in the energy converting process at the junction. The voltage factor depends on the base resisitivity and the intensity of the β-irradiation in that both of these effect V_{oc}. The voltage factor is obviously also effected by the choice of semiconductor because each semiconductor has a different E_g. For silicon P-N junctions irradiated by betas emitted from Pm^{147} $V_{oc}/E_g \approx 0.36$. This can be determined using equation (3-10) and values for I_g and I_o of 3×10^{-5} A amp/cm^2 and I_o of 1×10^{-11} amp/cm^2 which are found for N^+P silicon diodes used in energy conversion.

Factor (3), the curve factor, expresses the ratio of the maximum power available from the cell to the product of $I_{sc} \times V_{oc}$ and is given as C.F. = $I_m \times V_m / I_{sc} \times V_{oc}$. This factor is always less than unity due to the fact that the diode equation is an exponential, with the consequence that any rectangle inscribed within the curve must be smaller in area than an external rectangle with corners at I_{sc} and V_{oc}. The n value in the exponential, which has already been described further rounds the knee of the I-V curve making the curve factor even smaller than that for an ideal diode. The curve factor for an ideal diode is approximately 0.82 whereas experimentally for the beta cell it is 0.7. The effect of these

three factors is to reduce the cell efficiency to approximately 6.9%. Other lesser factors reduce the efficiency of the cell to approximately 5% or less[3]. Some of these factors are (1) betas which are reflected from the device surface and not absorbed, (2) poor collection efficiency; electrons and holes which recombine before reaching the junction. This effect becomes very important when the minority carrier diffusion length becomes shorter than the penetration depth of the beta particles. (3) (3) resistance losses -- both series and shunt effects, (4) self-absorption of betas in the promethium oxide. This effect becomes larger the thicker the layer becomes which increases power output but lowers efficiency as the self-absorption increases. The efficiency is known to peak and begin to decrease around 2 mg/cm^2[8].

CHAPTER IV

THE EPITAXIAL GROWTH SYSTEM

4.1 Introduction

It has been shown that large area junctions, grown epitaxially, are superior in terms of higher breakdown voltages and lower reverse saturation currents, to the diffusion technique for the fabrication of large area shallow junctions.[7] For this reason it was decided to use an epitaxial growth process to study the energy conversion by silicon P-N junctions of a radioactive beta emitter.

The epitaxial growth of silicon can be achieved in a gas flow system by the thermal reduction of silicon halides and the pyrolysis of silane. The silane process in a flow system has been reported by Bhola and Mayer[19]. The relative merits of this process over the commonly used tetrachloride process are fairly well established. The pyrolysis is thermochemically and kinetically more favourable than the thermal reduction of silicon tetrachloride or silicon trichloride. Silane is thermochemically unstable at room temperature and above and decomposes rapidly above 600^{o}C thus enabling the growth of silicon at lower temperatures. The use of a lower substrate temperature not only reduces the amount of diffusion between adjacent layers of silicon but also minimizes

the liberation of impurities from the susceptor used for heating the substrates and also allows for less diffusion of lifetime killing impurities into the substrate. Furthermore, the pyrolysis of silane is essentially chemically irreversible; the undesirable consequences of chemical transport associated with the silicon halide processes may be eliminated and the resistivity of the epitaxial layer may be better controlled. On the other hand, the silane process has the disadvantage that the thermal instability of the silane tends to promote nucleation by pyrolysis in the gas phase. The solid silicon formed in the gas phase is in the form of large atomic clusters of random orientation, and the deposition of these clusters on the growing interface could interfere with the oriented growth. The gas phase nucleation, however, can be suppressed by optimizing experimental conditions[7].

It is important that oxygen, in particular, be eliminated from the system because traces of oxygen interfere with the doping and react with silicon to form silicon monoxide particles which can become imbedded within the deposit thus creating inhomogeneities in the crystal[20]. It is important that the crystal be free of any major defect because just one is sufficient to ruin the device to be fabricated.

Extreme care must be taken with pure silane as mixtures of silane and air are explosive over a wide range of composition. It has been found[19], however, that silane diluted with hydrogen or a rare gas to a concentration of less than 5% by volume is not pyrophoric.

The following section describes the chemical vapour deposition (CVD) system used to carry out the epitaxial growth with controlled

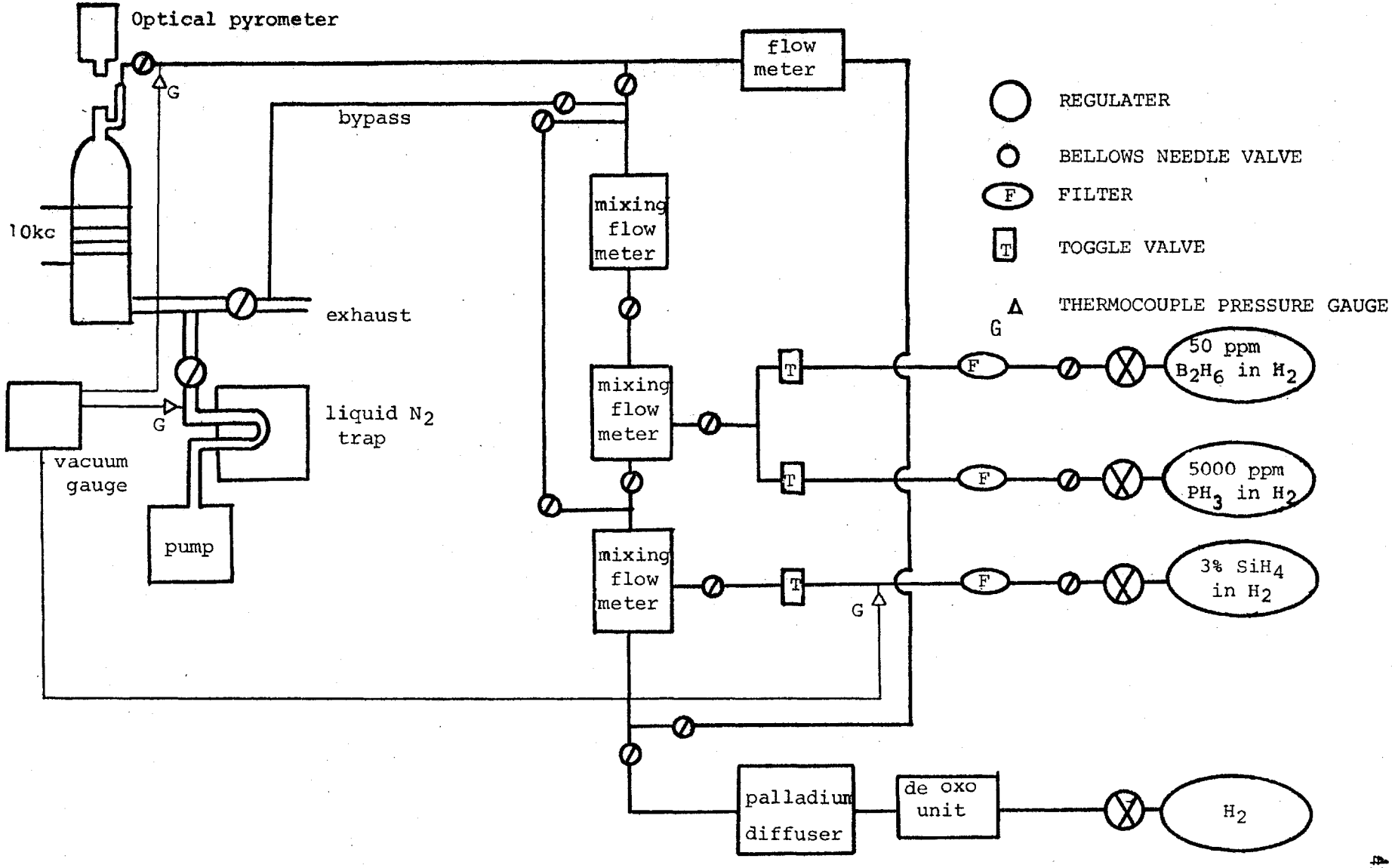

Figure 4-1 Flow diagram for the epitaxial growth system.

doping profiles.

4.2 The Chemical Vapour Deposition System

For reasons pointed out in the preceding section the epitaxial growth was carried out by the pyrolysis of silane using a gas flow system in a vertical reactor. The silane source was electronic grade 3% by volume of silane in hydrogen purchased from the Matheson Gas Company. The dopant gases, also electronic grade from Matheson, were 5,000 ppm phosphine in hydrogen and 50 ppm diborane in hydrogen. All reactant gases were passed through submicron filters to remove any solid particles before entering the main gas line. The hydrogen used as a diluent and carrier gas was ordinary hydrogen which was first passed through a deoxo unit and then a hydrogen purifier containing a palladium silver alloy purchased from Englehard Industries (with a capacity of 20 SCFH) before entering the main gas stream. The purifier was capable of delivering 20 SCFH of pure hydrogen. A schematic of the deposition system is shown in Figure 4-1.

All gas lines and valves of this system are made of stainless steel and connected with swagelock fittings with the exception of the reactor chamber and flowmeter tubes which have viton "O" rings. The flowmeters are single tube or mixing flowmeters purchased from the Matheson Company but fitted with Brooks "N.R.S." valves for better flow control. Before the system was put into operation it was checked for leaks by

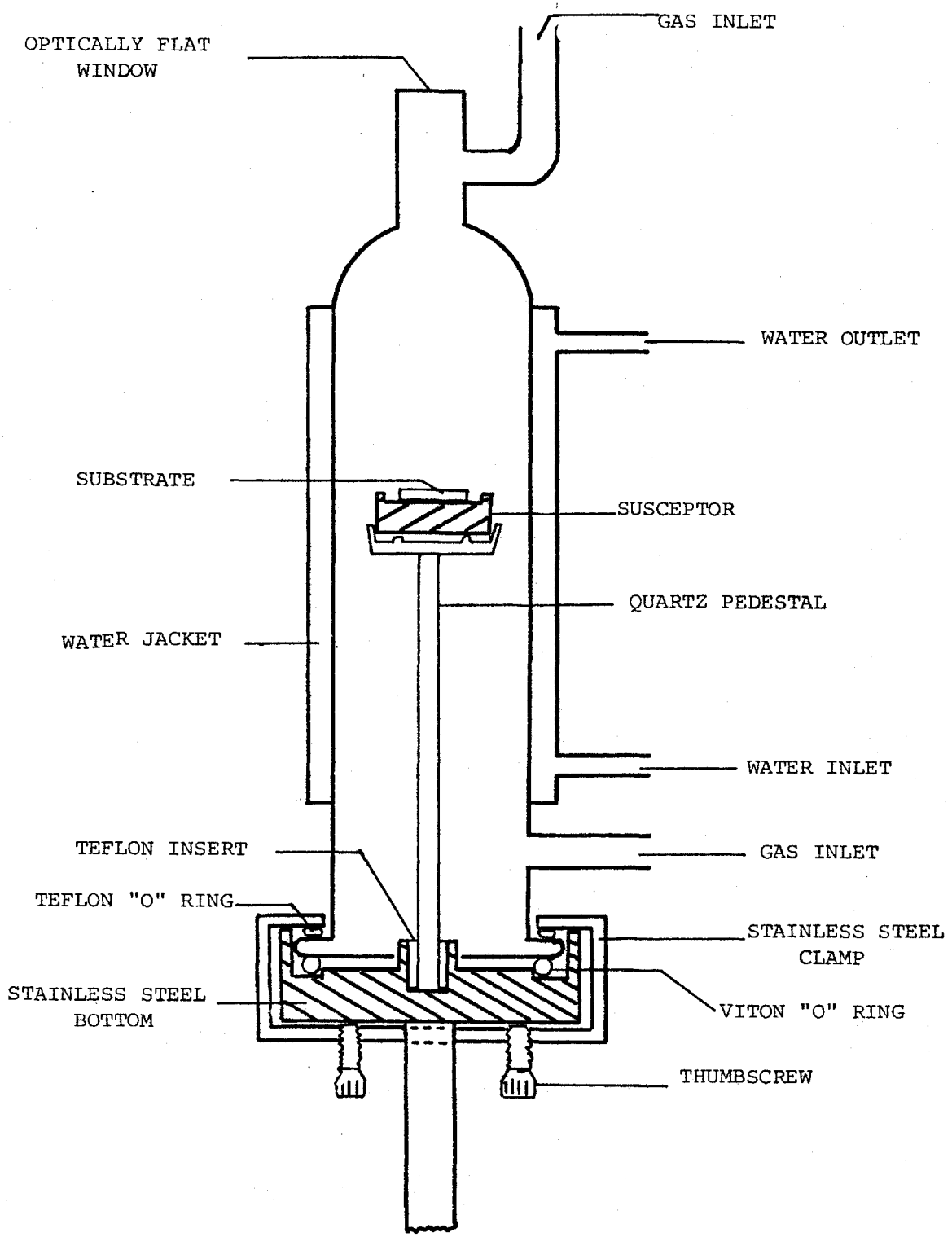

Figure 4-2 Detail of the growth chamber.

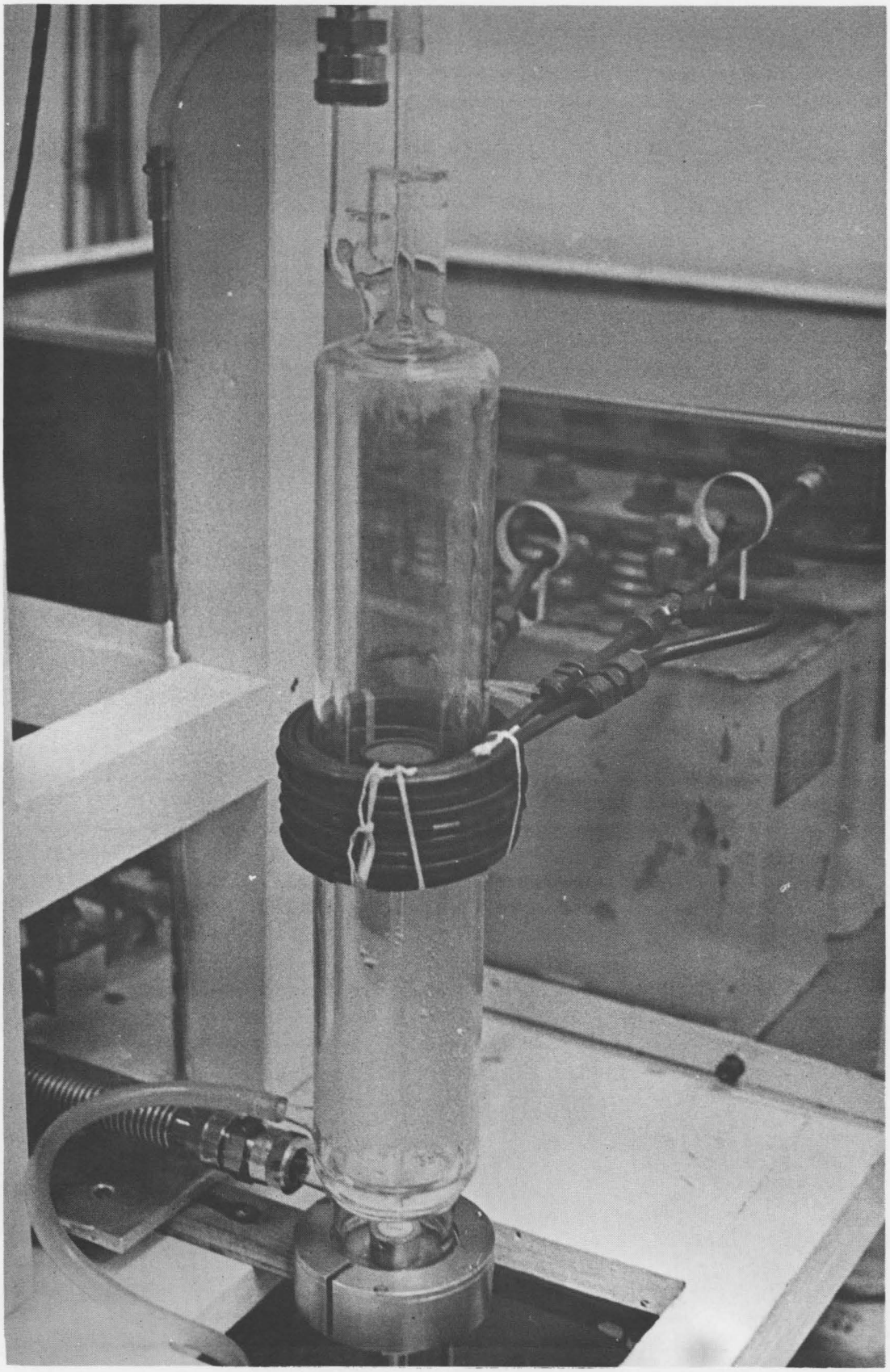

Fig. 4-3(a) Photograph of the chamber susceptor and induction coil mounted in position.

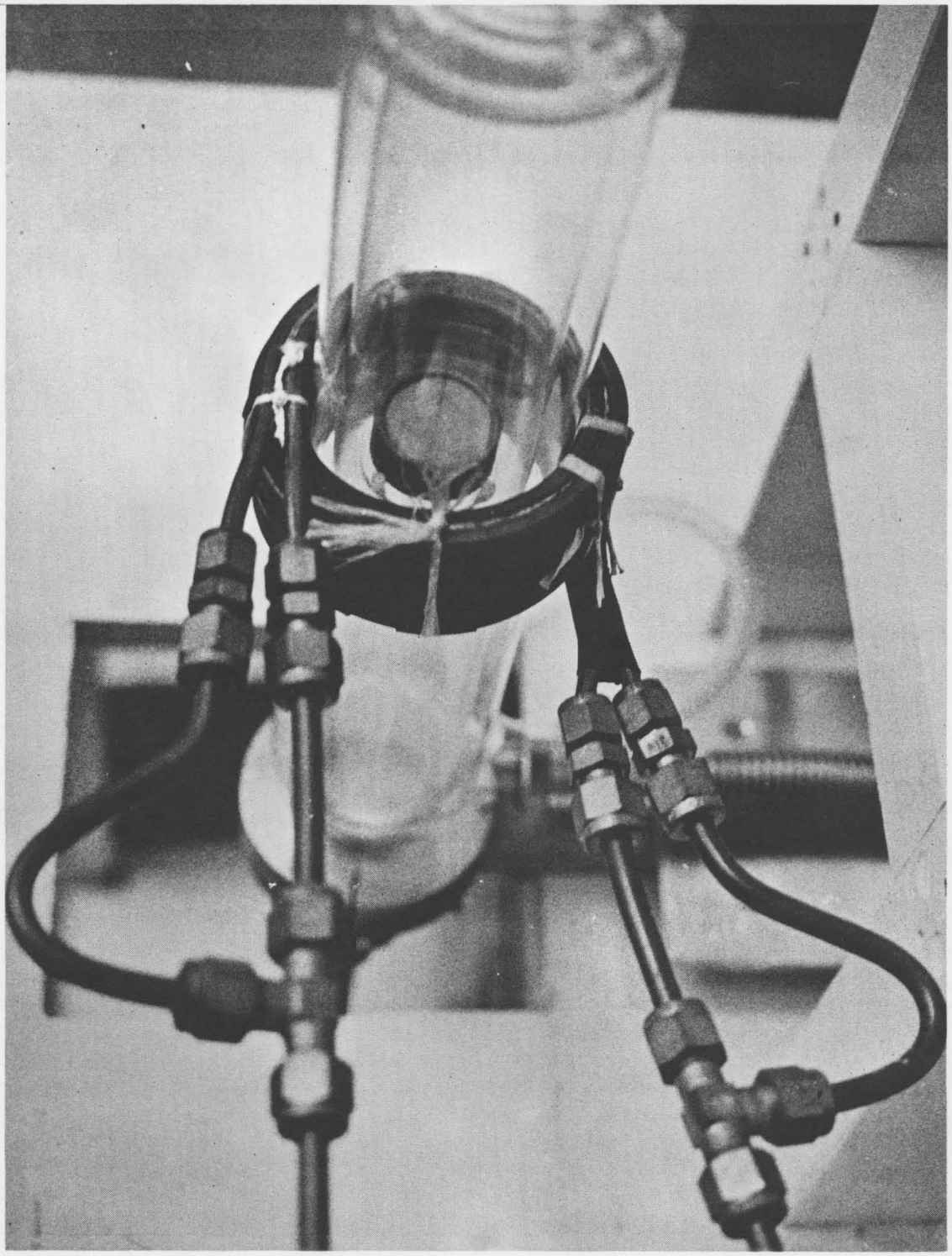

Fig. 4-3(b) Close-up of induction coil and susceptor.

evacuating the gas lines using a rotary pump and observing any changes in vacuum by the thermocouple vacuum gauges after the pump had been isolated.

The reactor tube is made of quartz with an inside diameter of 4 cm and held in a vertical position. A water jacket is used to keep the reactor wall cool so that the pyrolysis of silane is confined to the induction heated susceptor upon which the silicon substrates are heated. The susceptor is a silicon carbide coated graphite disk with a depression on one side. The disk is 0.5 in. thick and 1.13 in. in diameter. The depression is 30 mil. deep and 1 in. in diameter. The susceptor is supported by a quartz pedestal which fits into a teflon seat in the stainless steel bottom of the reaction chamber as can be seen in Figure 4-2. The entire stainless steel bottom is raised or lowered to load and unload samples.

The generator used to provide the induction heating did not operate at the higher frequencies of most generators commonly employed for epitaxial reactors. The generator operated at only 10 Kc and a power rating of 15 KVA. For this reason care had to be taken in constructing a coil which would provide a strong enough induction field to heat the susceptor. The coil itself is pictured in Figure 4-3. The coil is made of quarter inch copper tubing and is water cooled. The return temperature of the water is monitored to make sure the coil does not overheat. In order to obtain maximum coupling between the coil and susceptor the coil was connected in parallel to two tuning capacitors so that the maximum resonant frequency could be achieved. The temperature of the sample was

measured by means of a two color comparator pyrometer which operated at 0.55 and 0.65 micron wavelengths. The pyrometer was focussed onto the substrate through the optical window at the top of the reaction chamber.

CHAPTER V

EXPERIMENTAL

5.1 Introduction

In this chapter are presented the experimental techniques used in the epitaxial growth of the P-N junction devices and the methods of their evaluation. The growth covers sample preparation and the growth of both doped and undoped single crystal layers of silicon. The evaluation covers crystal perfection and doping profiles.

5.2 Substrate Preparation

The substrates upon which the epitaxial layers were grown were 10 mil. thick "monex" slices obtained from Monsanto. All slices larger than one inch in diameter were scribed into quarters so that they would fit onto the susceptor. The "monex" slices are "Syton" polished and no further polishing is necessary and the only preparation necessary is to remove any surface oxide and surface contamination, whether organic or metal ions. In order to achieve clean surfaces on which relatively defect free epitaxial layers may be grown several cleaning procedures were evaluated.

1) 10 minutes in hot H_2O_2:H_2SO_4 (1:1) plus rinse in D.I. water
10 minutes in hot H_2O:H_2O_2:HCl (4:1:1) plus rinse in water
5 minutes in hot dilute HF plus rinse in D.I. water
Call this procedure C1

2) C1 plus an insitu prefire in H_2 for 20 min. at 1100°C in the epitaxial reactor.
Call this procedure C1(a)

3) 30 second dip in 48% HF.
Call this procedure C2

4) 10 min. in hot dilute HF plus rinse in D.I. water
15 min. at 70-80°C in H_2O:H_2O_2:NH_4OH (5:1:1 to 7:2:1) plus rinse in D.I. water
15 min. at 70-80°C in H_2O:H_2O_2:HCl (5:1:1 to 7:2:1) plus rinse in D.I. water
15 min. at 70-80°C in H_2O:H_2O_2:HCl (8:1:1 to 8:2:1) plus rinse in D.I. water[21]
Call this procedure C3

5) C3 plus an "in situ" prefire at 1100°C for 20 min. in H_2
Call this procedure C3(a)

The dionized water was obtained using a super Q filtration system from the Millipore Corp. and delived water with a resistivity larger than 18 megaohms. The final step in all the cleaning procedures was to blow dry the substrates using helium.

The epitaxial layers grown on substrates using all the above cleaning procedures can appear mirror smooth and show no gross defects using a high intensity light as suggested by Lenie[34]. However, C2 does not always yield a mirror smooth surface whereas the rest do which suggests that the as-received substrates have some surface contamination.

Stacking fault densities as revealed by Sirtl[22] etching, vary according to the cleaning procedure with C1 yielding the largest number of faults while C2 and C3 yield considerably less. It was found that C1(a) reduced the number of stacking faults found using C1 by at least three orders of magnitude but still only a slight improvement from C2 or C3. Using C3(a) the defect density was reduced to between 10 and 100 per cm^2 at growth temperatures of 1070°C. Consequently procedure C3(a) was used for device fabrication.

5.3 Epitaxial Growth of Undoped Films

The general procedure used for the epitaxial growth of an undoped silicon layer is as follows:

(1) The prepared silicon substrate is loaded onto the susceptor which is then raised into the chamber so that the susceptor is in the middle of the induction coil.

(2) The thumbscrews are then tightened to obtain a vacuum "O" ring seal at the bottom of the chamber. The chamber is then evacuated using the rotary pump to remove the air and last traces of moisture.

(3) Hydrogen is admitted until atmospheric pressure is reached and then the exhaust is opened. The hydrogen flow is adjusted to 5 l/min. and the chamber flushed for thirty minutes.

(4) After the purge is completed the substrate temperature is raised to 1100^{o}C and kept there for 20 minutes.

(5) The temperature is adjusted to the growth temperature and while it is stabilizing the silane flow is adjusted to the desired flow rate for growth using the bypass directly to the exhaust without going into the reaction chamber.

(6) After the temperature is stable the bypass is shut off and the SiH_4/H_2 gas stream admitted into the reactor where the silane decomposes and silicon is deposited on the substrate.

(7) After the desired deposition time the silane flow is shut off; the temperature reduced at an initial rate of approximately 300°C/min., and the susceptor allowed to cool for 10 minutes in the hydrogen stream before the sample is removed.

As will be seen later only slight modifications are introduced when doping the grown epitaxial film to a given concentration.

Since it is desirable for the epitaxial layers used in device fabrication to be grown at as low a temperature and as fast a growth rate as possible in order to minimize any diffusion between layers or the diffusion of lifetime killing impurities, the optimum growth parameters commensurate with the above conditions was first established for crystal growth without intentional doping.

The growth rate and crystal perfection of silicon using silane epitaxial deposition systems has been established by many authors with respect to temperature, partial pressure of silane and total gas flow[8,23,24]. With the specific reactor design and dimensions of the epitaxial system which has already been described it was found that the optimum growth rate and temperature together with good quality crystal perfection were 0.7 microns per minute at 1050°C. The total gas flow was 5.5 l/min. and the silane concentration 0.13%. Increased silane concentrations lead to polycrystalline or amorphous layers whereas decreased concentrations lead to slower growth rates. Decreasing temperature also leads to films of poor quality.

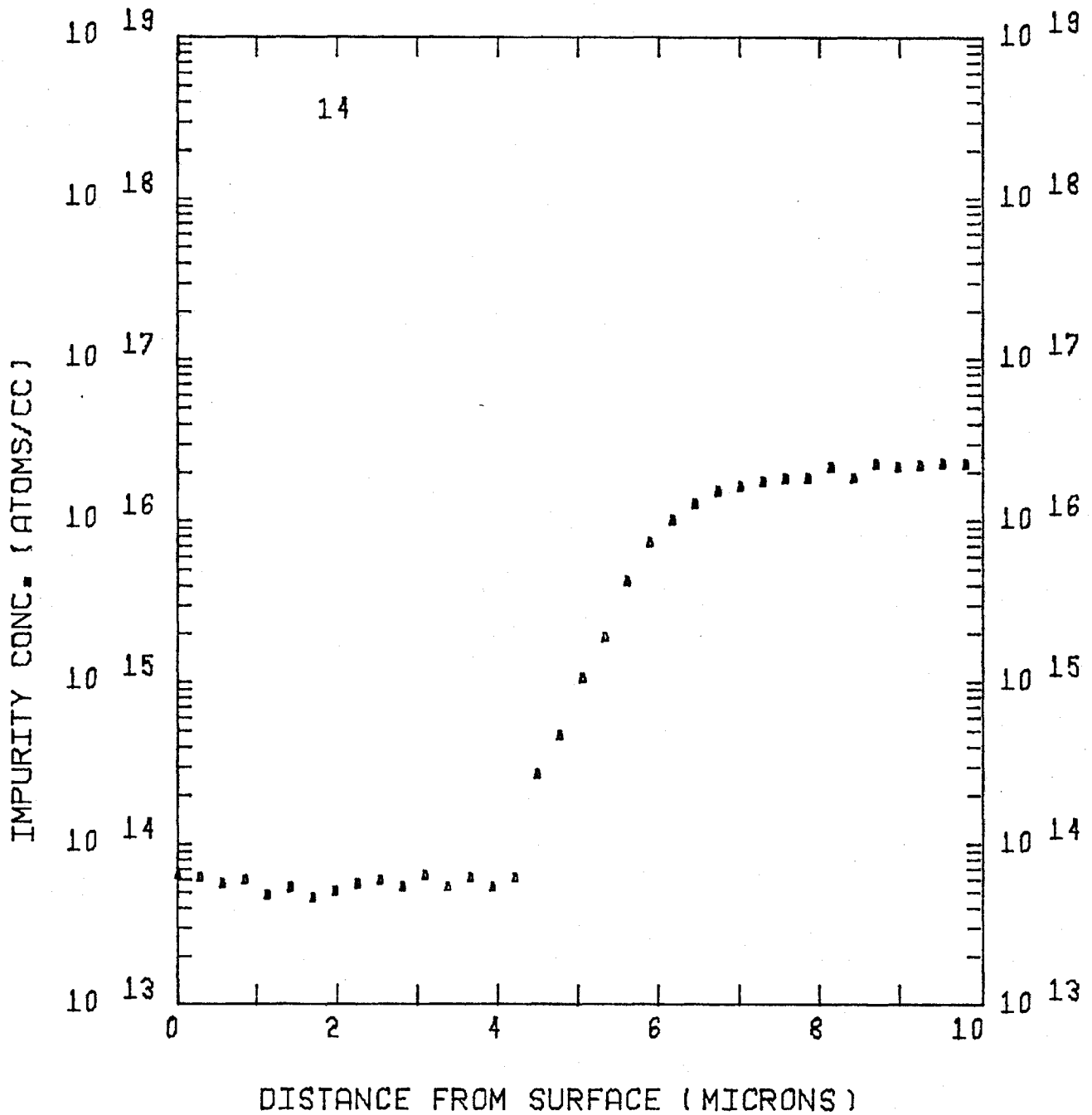

Figure 5-1 Concentration profile of a low doped n-type growth on an n-type substrate as determined from spreading resistance probe measurements.

(a)

Si <100> substrate

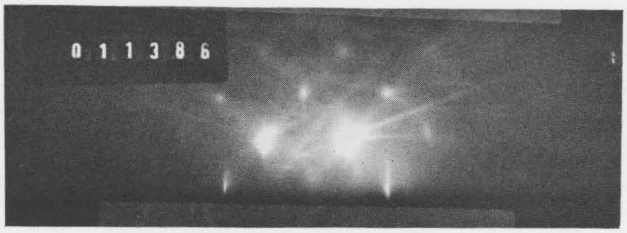

(b)

Si <100> Film

Fig. 5-2. High energy electron reflection diffraction patterns of (a) Si <100> substrate (b) Si <100> Film

The resistivity of the undoped epitaxial layers was approximately 100 Ω cm n-type as determined from spreading resistance probe measurements. This probe, model ASR-100, was obtained from Solid State Measurements Inc. and is similar to that described by Mazur and Dickey[25]. The profile of an n-type layer on an n-type substrate is shown in Figure 5-1.

It has already been stated that the grown layers were mirror smooth and had relatively low defect densities. The crystallinity of the layer was also evaluated using high energy electron reflection defraction which yielded single crystal patterns identical to the substrates. This is illustrated in Figure 5-2 where the spot pattern and strong Kikuchi lines are indicative of the crystal perfection.

5.4 Doping of Epitaxial Films

It has already been stated that for high efficiencies in the direct energy conversion of the incident beta particles by the P-N junction it is desirable to have both the n- and p-type regions highly doped in order to obtain a large built in potential. Also it is necessary to have long minority carrier lifetimes in both regions of the junction so that maximum collection of electrons and holes may be achieved. It has also been pointed out that the lifetime degrades with the level of impurities introduced into the semiconductor. For these reasons the ideal junction for energy conversion is a one-sided abrupt junction with the heavily doped layer forming a shallow junction[16]. It has also been

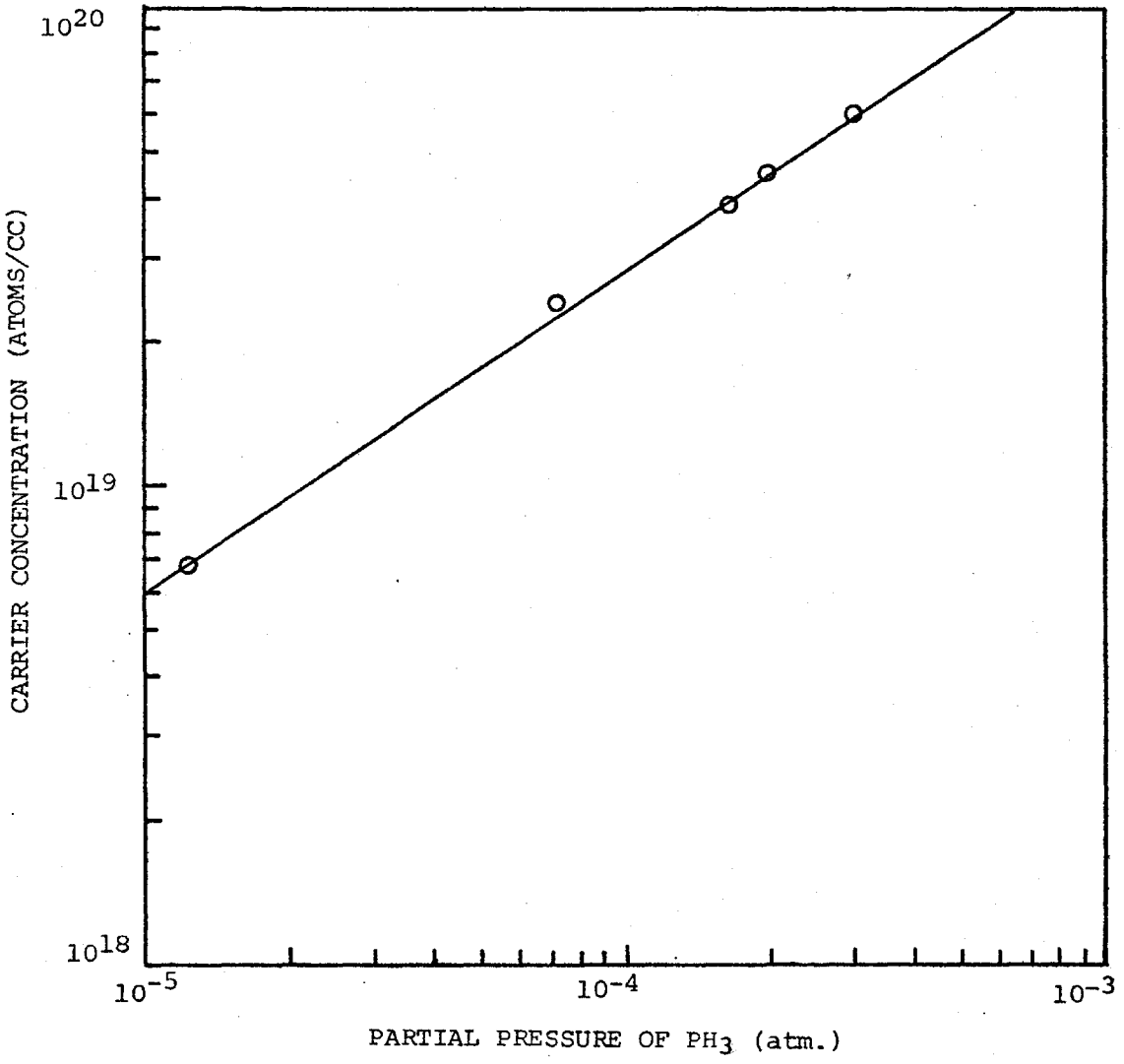

Figure 5-3 Graph of the partial pressure of PH_3 in the deposition gas versus the carrier concentration in the grown layer.

shown[26] that N^+P junctions are more radiation resistant than P^+N cells and therefore N^+P cells will have a longer lifetime. For this reason N^+P junctions were fabricated for the direct energy conversion of beta particles emitted from Pm^{147}.

In order to obtain a N^+ layer phosphine from the 5000 ppm in ultrahigh purity H_2 source was added to the silane flow in steps (5) and (6) of section 5.3. In step (6) the silane and phosphine are added simultaneously using on/off toggle valves to the H_2 carrier gas. The partial pressure of silane in all doping runs was 1.3×10^{-3} atm, resulting in a growth rate of 0.7 microns per min. at 1050°C. A plot of the partial pressure of phosphine vs. the doping concentration in the grown epitaxial layer is shown in Figure 5-3. The partial pressure of the dopant gas is proportional to its concentration in the hydrogen carrier stream since the hydrogen is at 1 atm. in the reaction chamber.

The N^+ epitaxial films were grown on p-type boron doped substrates. The impurity profiles were determined by spreading resistance probe measurements which were complimented with Hall effect measurements from which the average concentration of the grown film can be determined. A typical profile of an N^+P junction is shown in Figure 5-4. The Hall effect measurements were performed at room temperature using the method of Van der Pauw[27]. Employing suitable masking techniques Van der Pauw clover leaf patterns were mesa etched in the deposited layer. By applying a reverse bias the pattern could be electrically isolated from the substrate. Conductivity and Hall effect measurements performed on these isolated patterns allowed the resistivity, carrier concentration and mobility in

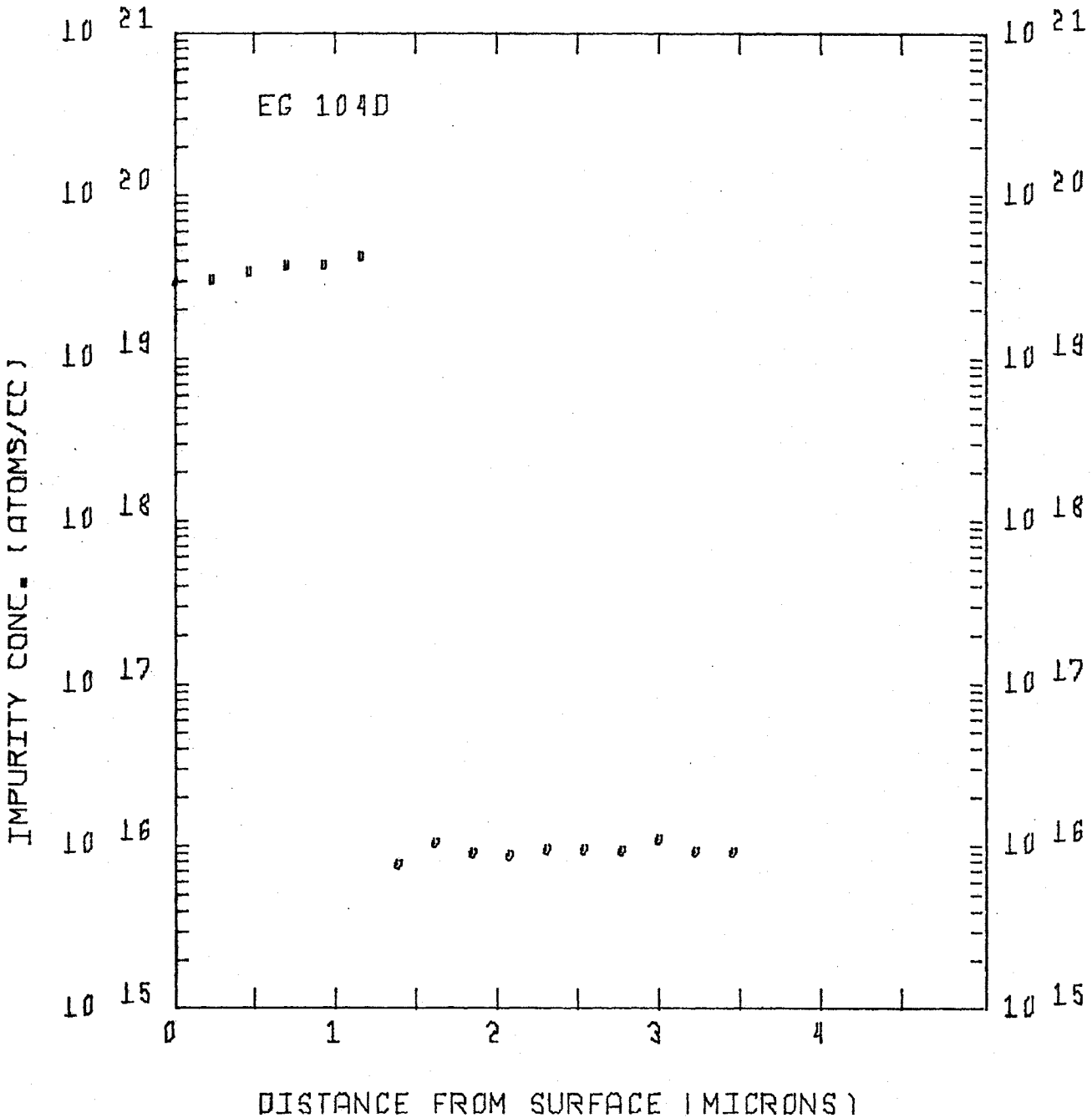

Figure 5-4 Concentration profile of an N^+ grown layer on a p-type substrate as determined from spreading resistance probe measurements.

the deposited layer to be determined. Both the techniques employed to delineate these patterns and the subsequent electrical measurements are described in Appendix B.

The results of several layers of different dopant concentration are presented in Table II and compared to the conductivity mobilities of bulk material of the same concentrations. The Hall mobility, μ_H, is related to the conductivity mobility, μ_c, according to the relation $\mu_H = r\mu_c$[28] where r is dependent on the impurity concentration. For the high concentrations of the deposited layers in Table II r has a value of unity[28]. Therefore the conductivity mobilities of the grown layers are the same as those of bulk crystals indicating the high degree of crystal perfection of the grown film. Electron reflection diffraction patterns of the doped layers were identical to those of Figure 4-2 also indicating the crystalline perfection.

During the growth of epitaxial crystals using 0.13% silane in hydrogen without any doping intentionally added to the deposition gas stream only a slight deposit was noticed to build up on the reactor walls in the region of the susceptor or downstream in the chamber after long periods of growth. However, with the addition of phosphine to the gas flow a brown film was deposited on the reactor walls in the region of the susceptor and downstream from it. The amount of deposit increased as the partial pressure of the phosphine was increased. It was discovered that after the deposit became thick enough following runs resulted in poor crystal growth. This point was reached after a single run of one minute at a PH_3 pressure of 3×10^{-4} atm. or four to five runs of 1.5 minutes each at a PH_3

TABLE II

Comparison of Film Mobilities to Bulk Crystal

Doping Concentration (atoms/cc)	Hall Mobility (cm^2/volt-sec)	Film Conductivity Mobility (cm^2/volt-sec)	Typical Bulk Conductivity Mobility (cm^2/volt-sec)
1.8×10^{19}	94	94	94
2.4×10^{19}	86	86	88
3.8×10^{19}	81	81	79

pressure of 1.8×10^{-5} atm. This problem may possibly be overcome by constructing a reaction chamber with a larger inside diameter.

Due to present system limitations the maximum dilution of the phosphine gave a controlled doping density of 6.5×10^{18} atoms/cc.

Once the controlled doping of n-type epitaxial layers by the addition of PH_3 had been characterized diborane (B_2H_6) was incorporated into the system to add a p-type dopant to the grown layer. For subsequent device fabrication as has been described earlier, p-type doping was desired from degenerate doping down to 10^{16} atoms/cc.

As has been described earlier the diborane source was 50 ppm B_2H_6 in H_2. The diborane is added to the H_2 carrier gas along with the SiH_4 so that the total gas flow is 5.5 l/min. in steps (5) and (6) of the growth procedure exactly as the phosphine was added to obtain the n-type doping. At a partial pressure of 4.6×10^{-6} atm corresponding to a diborane flow rate of 510 cc/min. the p-type doping in the epitaxial layer was 1.3×10^{20} atoms/cc. The Hall mobility of a 1.2 micron layer doped to 1.3×10^{20} atoms/cc was found to be 43.5 cm^2/volt-sec, as determined from Van der Pauw measurements, as opposed to a bulk conductivity mobility of 50 cm^2/volt-sec[28]. At this concentration r is unity and therefore the boron doped layer has a mobility 87% of a bulk crystal indicating that the degree of crystallinity in the grown layer is still high. The lower limit of controlled boron doping was found to be 1.4×10^{18} atoms/cc at a partial pressure of 1.3×10^{-7} atm corresponding to a diborane flow rate of 13.5 cc/min. Further dilution of B_2H_6 with the present system was unable to be achieved. A graph of the partial pressure of B_2H_6 vs. the dopant

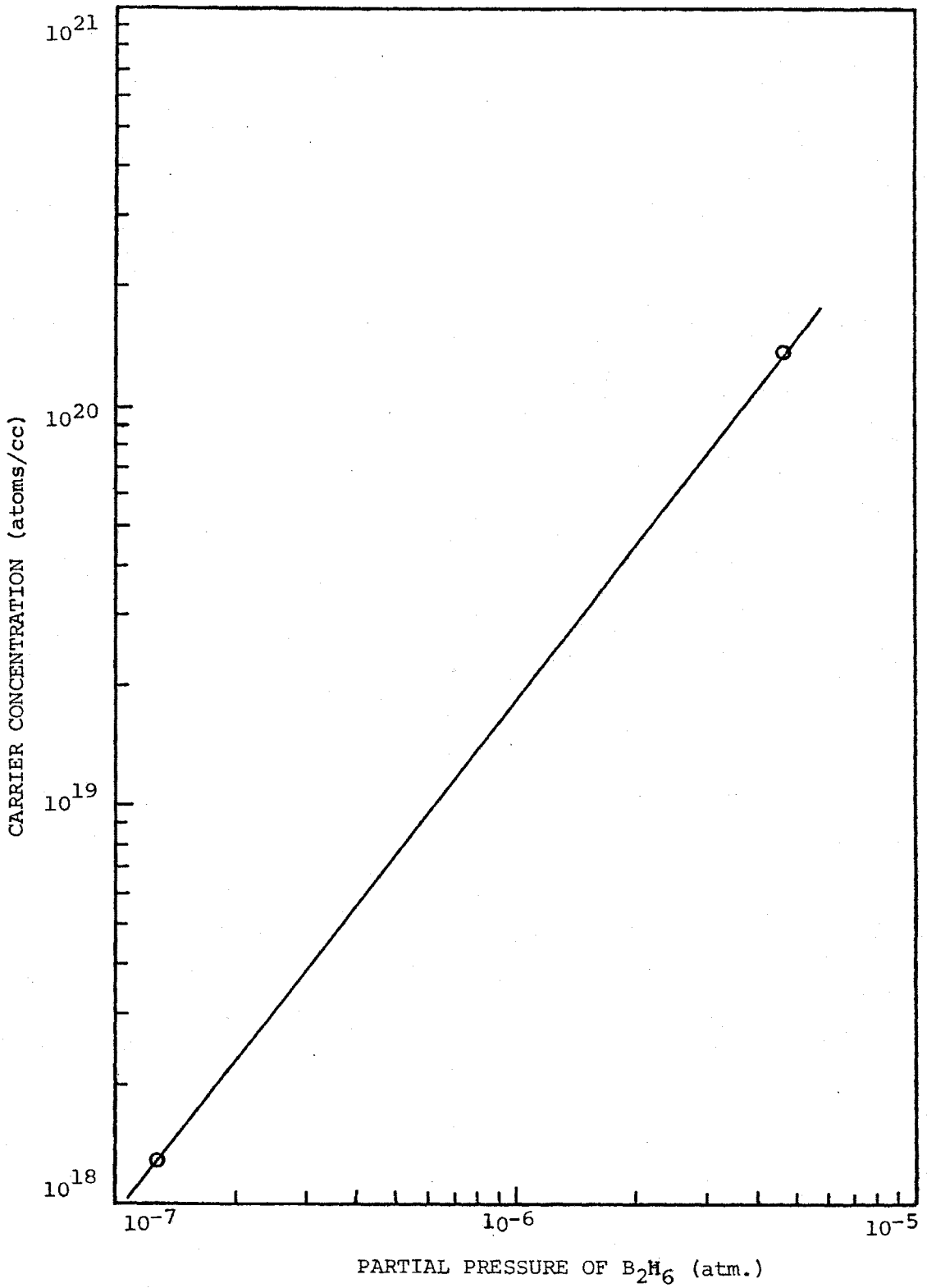

Figure 5-5 Graph of the partial pressure of B_2H_6 in the deposition gas versus the carrier concentration in the grown layer.

concentration in the epitaxially grown layer is shown in Figure 5-5. Although only two points were determined similar results for boron doping in the same concentration range carried out by P. Rai-Choudbury and E. I. Salkovitz[30] indicates that a straight line should join the two points.

5.5 Multilayer Epitaxial Growth

Once the controlled doping of both n- and p-type impurities had been achieved the growth of multilayered structures was attempted for use in energy converting diodes. The term multilayered here refers to the growth of a silicon crystal such that the doping type is changed or the concentration of the dopant type is altered as a function of crystal thickness. The growth of multilayered structures has been accomplished by many authors[35,36,37].

For reasons already discussed the desired structure was $N^+PP^+N^+P$ with the last P layer being the substrate. This structure is a three junction device and consists of four grown layers. The substrates used were 2 Ω cm (100) B-doped wafers. The procedure for cleaning and loading of the substrates into the reaction chamber and the growing of a single epitaxial layer has been discussed previously. The same procedure is followed for the growth of the first N^+ layer of the multilayer structure. Before the P^+ layer is grown the main gas line as well as the reaction chamber is flushed with hydrogen at a rate of 5 l/min. for 10 minutes.

In order that as little diffusion as possible occurs during the flushing, the power to the induction coil is turned down, but not off, so that the temperature of the substrate is considerably reduced (< 700°C). During the last 5 minutes of the hydrogen purge the silane and diborane flow rates are adjusted to the values which are desired during the growth of the P^+ layer. After the flush is completed the substrate is raised to the growth temperature (1070°C) in a hydrogen ambient. After the temperature has stabilized the silane and diborane are simultaneously turned on using toggle valves; the flow rates being preset during the preceding purging. After the desired layer thickness is grown the silane and diborane flows are simultaneously shut off.

The next layer to be grown is p-type which was desired to be approximately 1 Ω cm or 10^{16} atoms/cc. As has previously been noted, however, the lower limit of the controlled boron doping was found to be 1.4×10^{18} B atoms/cc - two orders of magnitude larger than that desired. In order to obtain low doped layers after the growth of the P^+ layer it was necessary to flush the main gas line and reaction chamber for one hour with hydrogen at the rate of 5 l/min and then grow the next layer using only silane and no intentional doping. During the flushing period the substrate temperature was again lowered and then raised to the growth temperature at the end of the purge. When the growth temperature had stabilized silane was turned on until the desired layer thickness had been achieved and then turned off using the toggle valve. Using this procedure P layers between 0.5 and 1.0 Ω cm p-type were produced. The p-type doping comes from residual boron doping in the chamber and gas lines. The

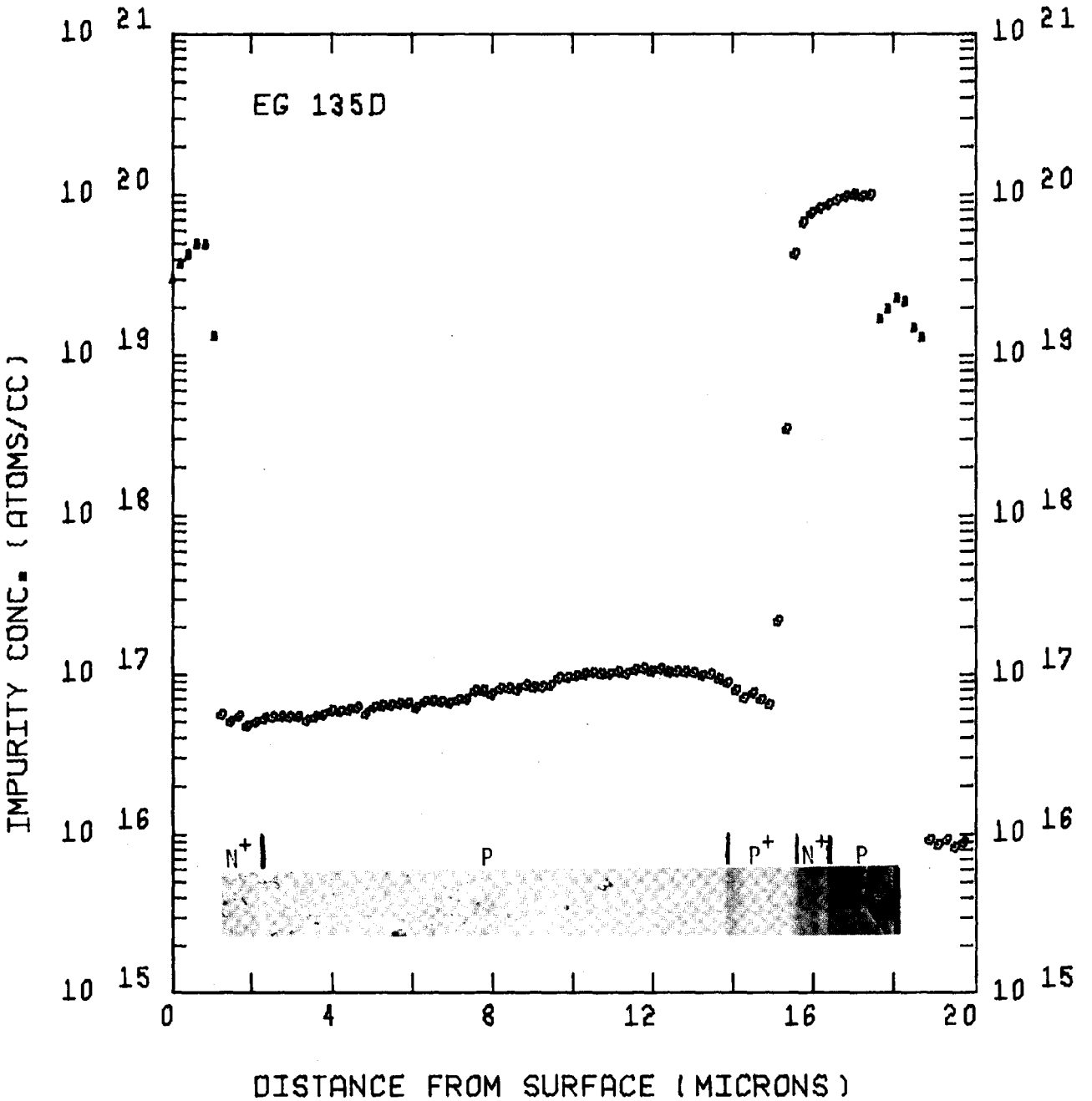

Figure 5-6 Concentration profile of an $N^+PP^+N^+$ epitaxial structure grown on a P type substrate as determined from spreading resistance probe measurements.

temperature of the substrate is lowered and the system is purged for 5 minutes with a hydrogen flow. During the final two minutes of this flush the PH_3 and SiH_4 flow rates are adjusted to the values desired during the growth of the second N^+ layer and then shut off. The substrate is again raised to the growth temperature and the N^+ layer is grown by turning on the PH_3 and SiH_4 flows simultaneously using the toggle valves. At the end of the growth period the PH_3 and SiH_4 flows are shut off and the sample allowed to cool in hydrogen for 10 minutes before it is removed from the reaction chamber.

An impurity profile for an $N^+PP^+N^+P$ structure as determined from spreading resistance probe measurements is presented in Figure 5-6. Also shown is a stain of the structure clearly showing all the different layers.

5.6 Summary

Using the epitaxial process it has been shown that both single junction and multijunction structures can be fabricated which should prove useful as direct energy converters. It should be noted that no additional sample handling is required for the multijunction structure than the single junction one and therefore device yields should be similar.

The method used at present to obtain a low doped layer after a highly doped layer has been grown (i.e., P on P^+) is far from satisfactory.

Considerable improvement should be achieved if individual doping sources and gas lines were used for high and low doping of impurities. To obtain low doped material it is recommended that a double or even triple dilution of the source gas be used.

When using epitaxial systems it is recommended that all gas lines always be pressurized and that after any shut down, whether only a day or two, considerable flushing of all gas lines be performed before any crystal growth be attempted.

CHAPTER VI

RESULTS AND DISCUSSION

6.1 Introduction

This chapter presents the electrical properties of the devices fabricated for direct energy conversion using the electron voltaic effect. The effects of various cell parameters such as series and shunt resistance, resistivity, and thickness of the grown layers are discussed.

6.2 Single Junction Devices

Employing suitable contacting and masking techniques large area circular mesas were etched into the grown layers and evaluated for their current-voltage relationships as described in Appendix B. A typical dark I-V characteristic for an N^+P diode is shown in Figure 6-1. The N^+ layer is doped to 4×10^{19} atoms/cc and the junction depth is 0.9 microns. The forward biased curve contains two regions of different slope. For small biasing the curve has n = 1.68 and for larger biasing n = 1.1 where n is contained in the exponential term of equation (2-4). This indicates that the current is dominated by generation-recombination (n = 2) in the low voltage regions but becomes highly diffusive (n = 1) for higher injection

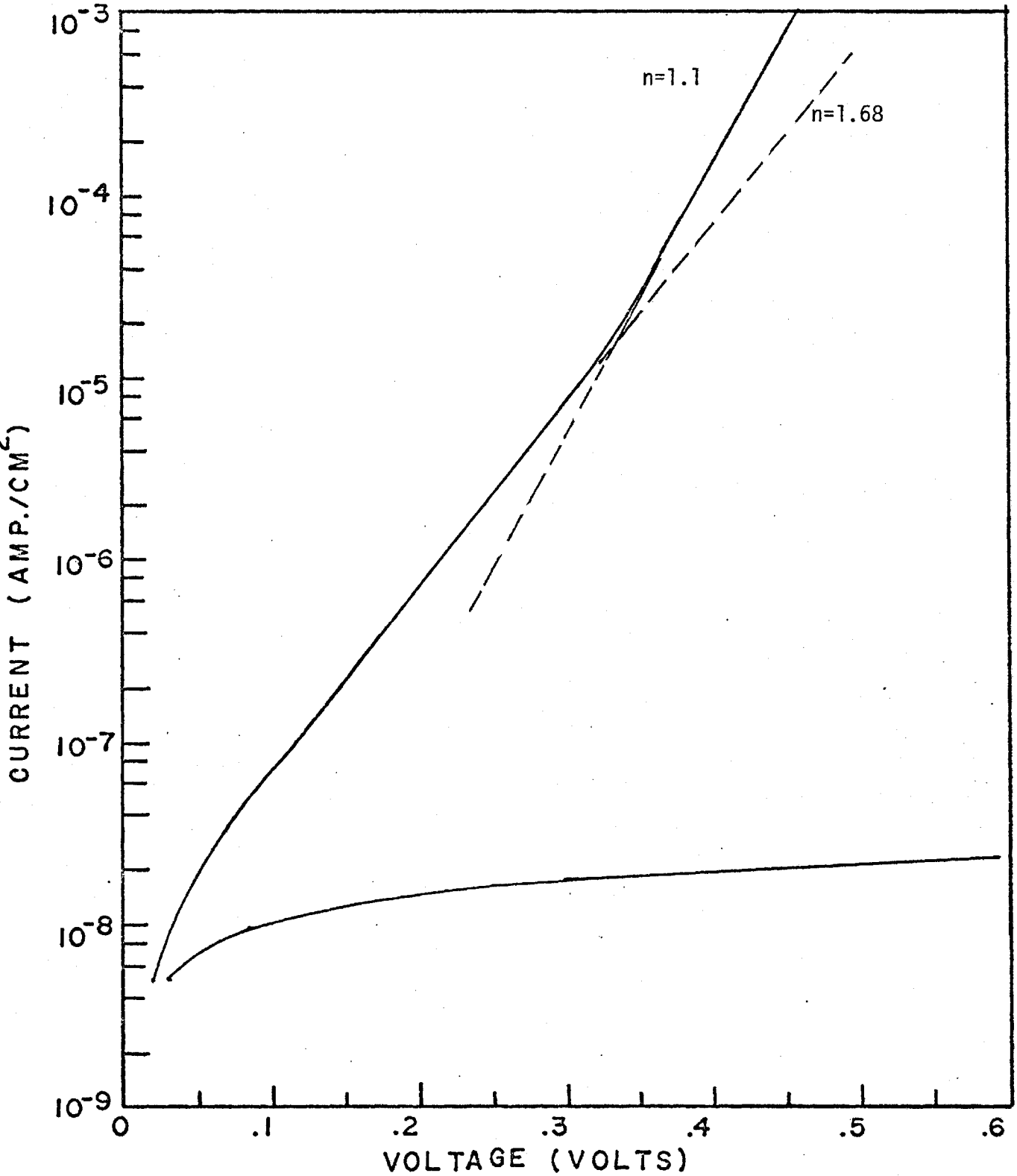

Figure 6-1 Semi-log plot of the current-voltage characteristics of a 1 cm^2 area unpassivated mesa diode with sintered Ti-Ag and Al contacts.

levels[10]. These values of n may be compared to those of solar cells in which n > 2 for even higher injection levels (0.4 - 0.5V)[16] than the n value of 1.68 shown in Figure 6-1.

The shunt resistance of the diode in Figure 5-1 is very large (greater than one megaohm as determined from the initial slope of the forward bias I-V curve) and has little effect on the forward characteristic beyond a bias of 0.1 volt. This value of shunt resistance is approximately two orders of magnitude larger than that reported by Wolf for solar cells[16]. Whereas for solar cells the smaller shunt resistance is tolerable due to the large generation currents obtained from solar irradiation, a shunt resistance of 10 kΩ would have a disastrous effect on the power output of a beta-voltaic cell due to the smaller generation currents.

A similar situation occurs for the series resistance effect on the beta-voltaic and photo-voltaic cells. Due to the lower generation currents obtained in the beta cell a larger series resistance can be tolerated than in the solar cell where higher current levels are obtained. In the case of a solar cell the series resistance should not exceed 0.5 Ω at most[17], whereas due to the lower generation currents of the beta cell the series resistance may be more than an order of magnitude larger than that used in solar cells. The effect of a large series resistance on the I-V characteristic similar to that in Figure 6-1 is shown in Figure 6-2 where the device contacts are made of unsintered aluminum. In this case the forward current deviates from the expected slope of the curve (n = 1.1 as determined using low resistance Ti-Ag contacts) at relatively low injection levels.

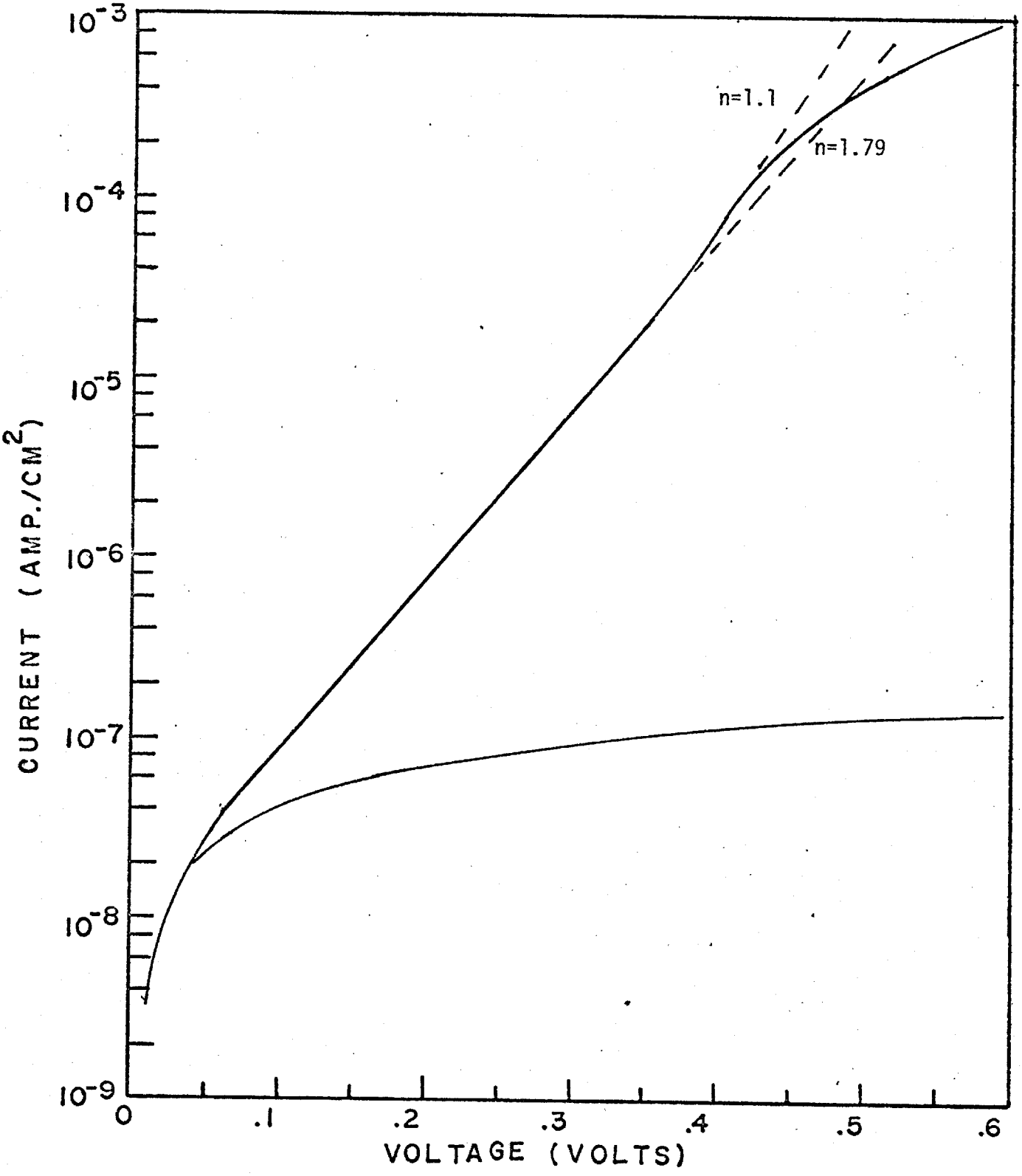

Figure 6-2 Semi-log plot of the current-voltage characteristics of a 1 cm^2 area unpassivated mesa diode with unsintered Al contacts.

However, it will be shown that for the intensity of the radiation used, the series resistance does not appreciably effect the power output of the beta cell because the generation currents are less than the current levels at which the Al contacts effect the forward bias I-V characteristic.

In order to construct an efficient beta energy converter using a P-N junction various cell parameters such as junction depth and resistivity were examined with respect to power output. The short circuit current, open circuit voltage, and power outputs of the mesa diodes was measured by placing them in contact with a Pm^{147} radioisotope source as described in Appendix D. The results of several diode structures are presented in Table III which indicates that for a N^+ layer doped to 4×10^{19} atoms/cc an optimum junction depth is approximately one micron.

The variation of open circuit voltage with base resistivity follows that predicted by theory in that the lower the resistivity the higher open circuit voltage is obtained. However, the higher resistivity substrates used as the base had higher initial minority carrier lifetimes -- the lifetime being the same in microseconds as the resistivity in Ω cm according to Monsanto Corp. This indicates that higher short circuit currents should be obtained in diodes using high resistivity substrates (i.e., lifetimes). As seen in Table III this is not the case but rather N^+P diodes differing in construction only in base resistivity had nearly identical short circuit currents. Measurements of the minority carrier lifetime in finished cells were then made by injecting a pulse and observing the decay of open circuit voltage[31]. The minority carrier lifetimes from all cells were found to be in the range 2.5 to 3.5 μ sec. This indicates

Variations in I_{sc} and V_{oc} with substrate doping and Junction depth.

TABLE III

Substrate Doping (B atoms/cc)	Layer Doping (P atoms/cc)	Junction Depth (μm)	Short Circuit Current (amp/cm^{2}x10^6)	Open Circuit Voltage (volts)
2×10^{14}	3.8×10^{19}	0.9	28.8	340
2×10^{15}	3.8×10^{19}	0.9	29.3	357
1×10^{16}	3.8×10^{19}	0.9	29.0	370*
1×10^{16}	3.8×10^{19}	0.3	27.0	350
1×10^{16}	3.8×10^{19}	0.6	28.2	364
1×10^{16}	3.8×10^{19}	1.8	29.4	345

* Optimum values

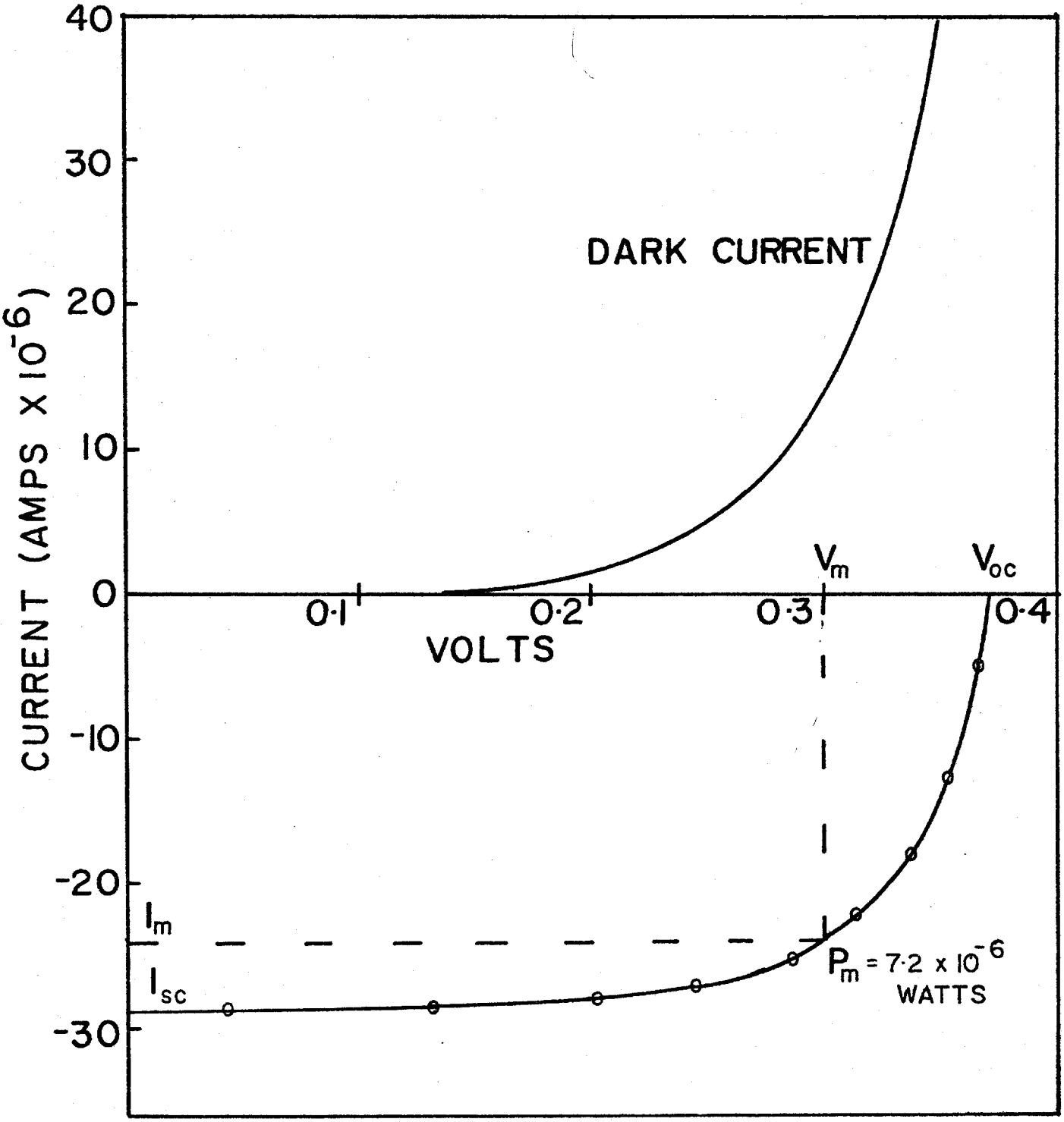

Figure 6-3 Plot of the current-voltage characteristics of a 1 cm^2 epitaxial single junction device when irradiated by Pm^{147}.

that the processing which the substrate undergoes reduces the effective lifetime to a maximum of 3.5 μ sec. The main factor causing this lifetime degradation is probably due to the elevated growth temperature used for the epitaxial growth process.

The power output from a typical N^+P cell with a 0.9 micron N^+ layer doped to 4×10^{19} P atoms/cc grown on a 2 Ω cm B doped substrate is shown in Figure 6-3. The device is one cm^2 in area and delivered a short circuit current of 29×10^{-6} amp. and an open circuit voltage of 370 mv. The maximum power obtained was 7.2 μ watts from a current of 24 μ amp at a voltage of 0.3 V. $P_m = 68\% (I_{sc} \times V_{oc})$. This is in good agreement with that obtained by Olsen et al[8] ($P_m = 70\% (I_{sc} \times V_{oc})$ for a 1 cm^2 phosphorous diffused diode in a 0.3 Ω cm boron doped substrate. While the P_m and I_{sc} of the epitaxial diode are larger than the value obtained by Olsen et al (5.2 μ watts and 20 μ amp) the open circuit voltages are nearly identical for diodes evaluated at 2 mg/cm^2 the source strength used in the present investigation.

6.3 Multiple Junction Devices

In this section are presented the results obtained from an investigation of the energy conversion properties of multilayer devices the growth of which has previously been described. It was anticipated that by fabricating such devices much larger open circuit voltages than single junction devices could be obtained while at the same time delivering a slight

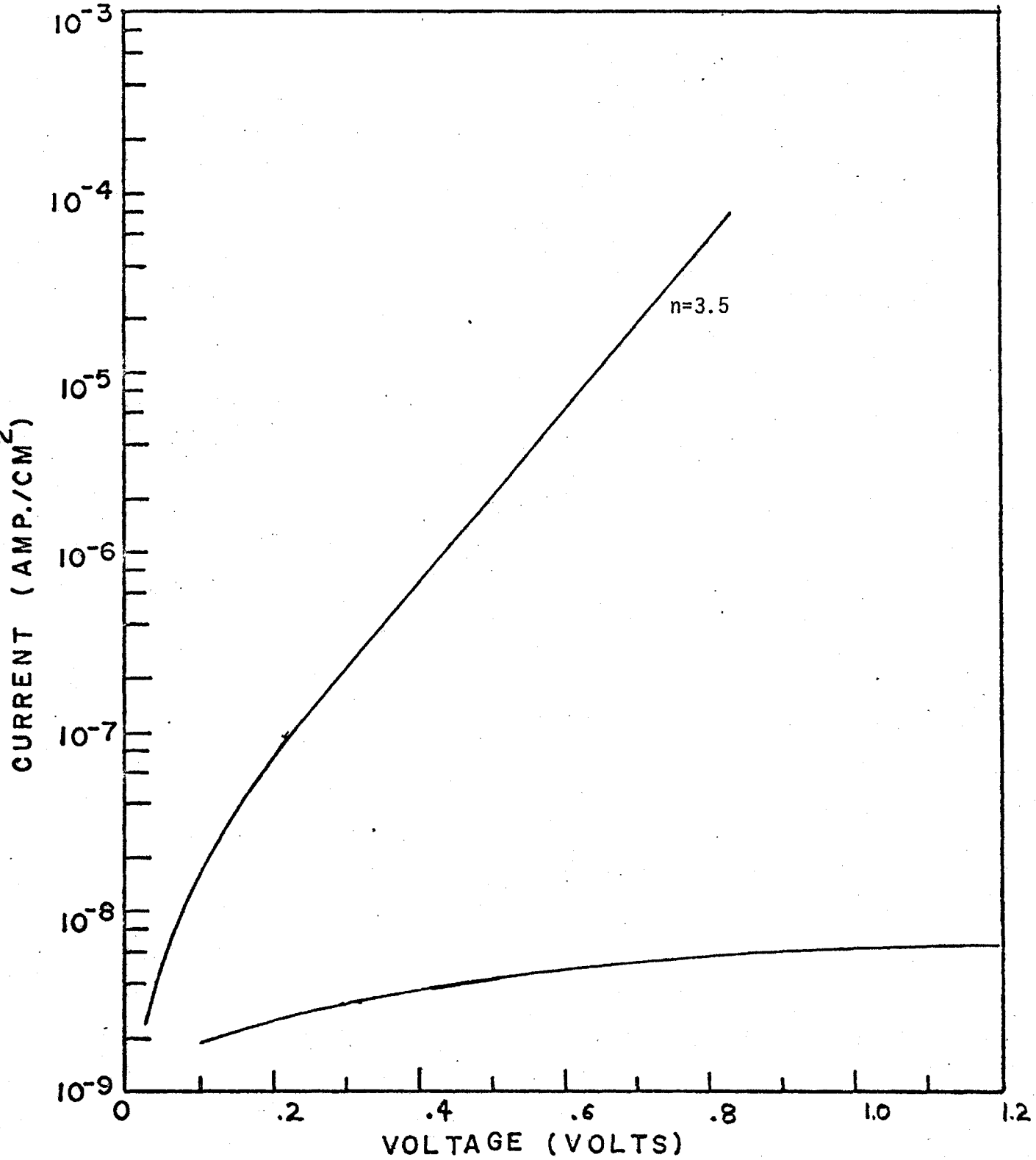

Figure 6-4 Semi-log plot of the current-voltage characteristics of an epitaxially grown device acting as two diodes in series.

increase in power output.

The forward dark I-V characteristics of a typical device with an $N^+PP^+N^+P$ structure are shown in Figure 6-4. As would be expected the n value for the straight line portion of the curve is 3.5 which is double that for a single junction (n = 1.68 - 1.79) and extends over twice the voltage range. Also for the same current level the bias voltage for the multilayer device is twice that for a single layer diode (i.e., 0.64 V compared to 0.32 V at 10^{-5} amp using Figures 6-2 and 6-4).

Since the current-voltage characteristics of the multilayer device were those of two diodes in series several devices were fabricated varying the thickness of the P and P^+ regions and evaluated as energy converters. The results are summarized in Figure 6-5. It can be seen that the optimum P^+ region for a doping of 10^{20} A atoms/cc should be 1 to 2 microns thick. This can easily be understood intuitively. It would be best to have the P^+ region as thin as possible to avoid beta absorption in this layer because electrons and holes created here do not contribute to useful power output. However, if the P^+ region is made too thin the recombination of minority carriers into majority carriers is not complete thus giving a poor ohmic contact between the two useful junctions.

The optimum thickness of the P layer is seen to be in the neighbourhood of 9.5 microns. This value is mainly due to the absorption of the beta particles by the silicon. In order to obtain the most efficient coupling between the two diodes each diode must develop the same generation current otherwise the output current of the device is limited to that of the

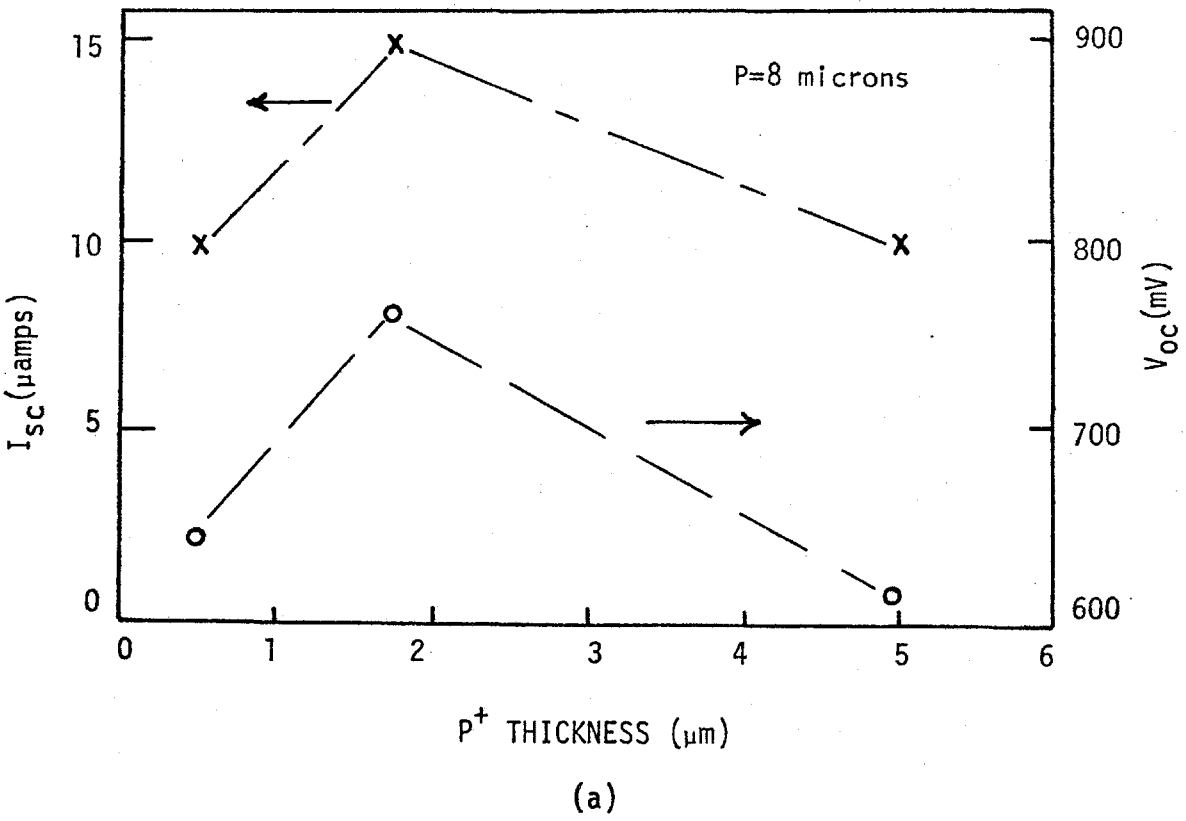

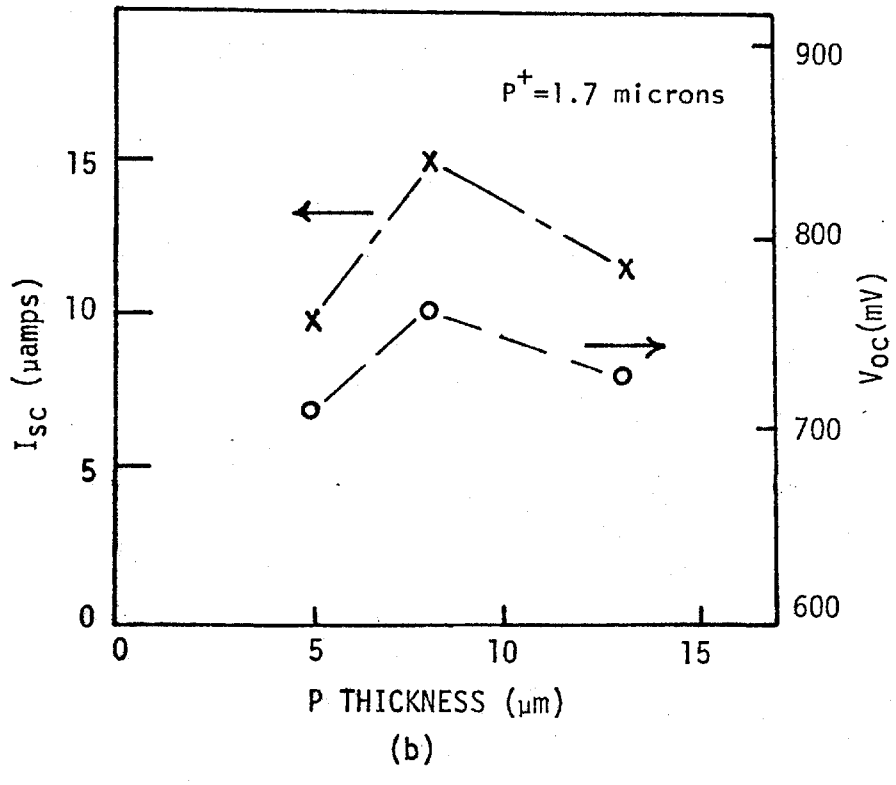

Figure 6-5 Graphs illustrating the optimum dimensions with respect to energy conversion of betas from Pm^{147} of (a) P^+ thickness, (b) P thickness for an $N^+PP^+N^+P$ structure which acts as two diodes in series.

poorer junction. Thus if the p-type region is too thin enough electrons are not collected by the junction and I_{sc} of the top junction is less than that of the bottom one. On the other hand, if the p layer is too thick most of the incident radiation is absorbed before it reaches the bottom junction and I_{sc} of this junction is lower than that of the top one. The optimum condition is reached when each junction absorbs equal amounts of radiation thus producing identical values for I_{sc} of the two junctions. Because of this the short circuit current for the multilayer device would not be expected to be much larger than that of a single junction for a given intensity of radiation. From a simple theoretical treatment of the $N^+PP^+N^+P$ diode given in Section 3.3 it was found that an optimum thickness for the P^+ region is approximately 1 micron and for the P region 13 microns. These values are in close agreement with those found experimentally (1-2 μm for P^+ and 9.5 μm for P), considering the complexity of the device and the assumptions made in determining the theoretical values.

A typical diode with near optimum dimensions for the P and P^+ regions is shown in Figure 6-6. For this 1 cm^2 multilayer diode the P layer was 7.5 microns and the P^+ layer 1.7 microns. The short circuit current is 15.2 μ amp and the open circuit voltage 763 mV. The maximum power was 8 μ watts obtained from a voltage of 0.6V and a current of 13.3 μ amp. P_m = 70% (I_{sc} x V_{oc}) and is approximately the same percentage as for a single junction device, although an overall increase in power output of 11% is achieved. Part of this increase arises from the fact that V_{oc} of

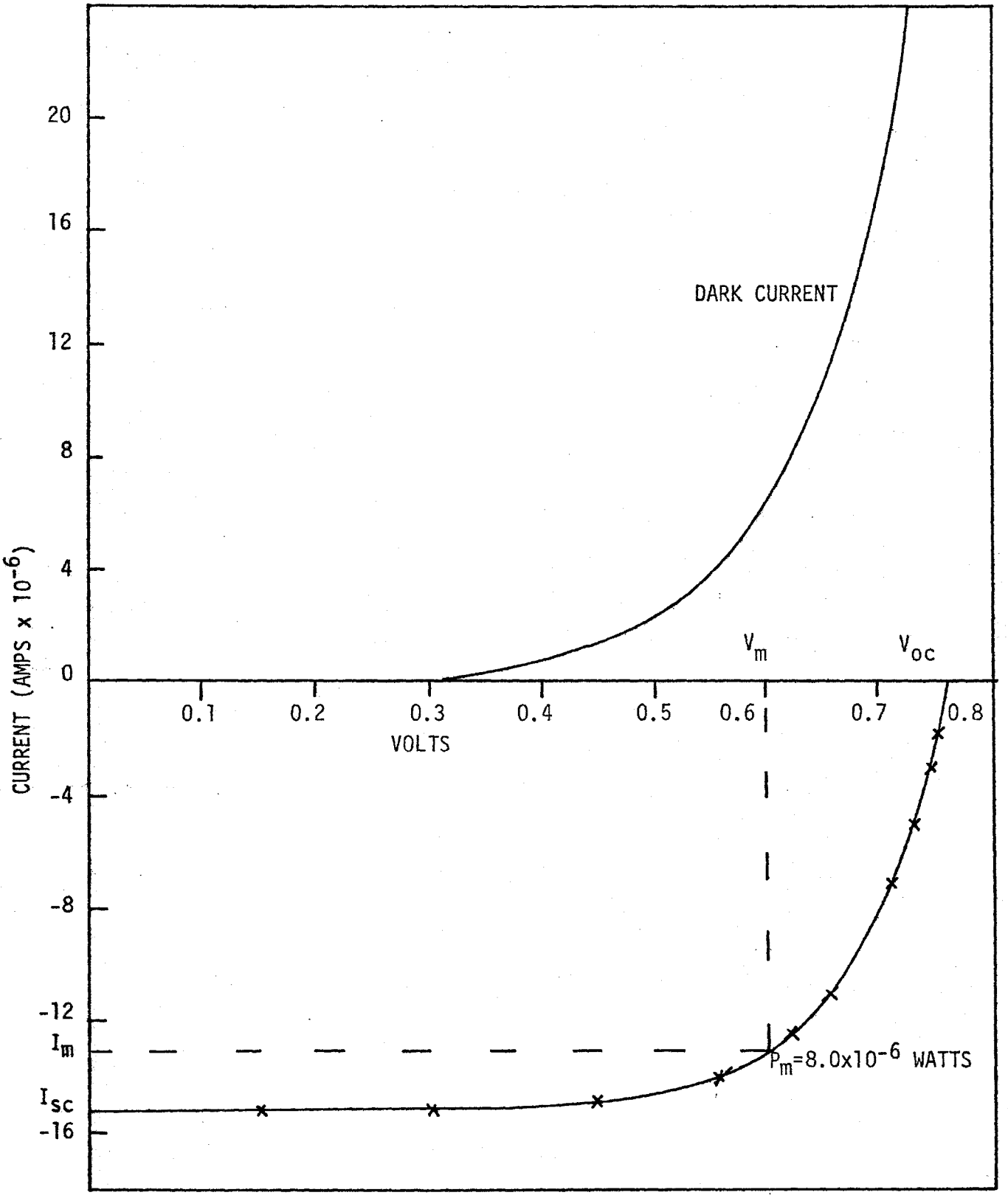

Figure 6-6 Plot of the current-voltage characteristics of a 1 cm^2 area $N^+PP^+N^+P$ device acting as two diodes in series when irradiated by Pm^{147}.

the multilayer structure is slightly more than double V_{oc} for a single diode. This increase ispartially obtained in the top diode of the structure where the P-type doping of the base region is larger than 10^{16} atoms/cc, the substrate concentration, thus giving the overall device a higher V_{oc} than would be expected for a symmetrical structure. Most of the increase, however, is found in the short circuit current which is larger than half the value of I_{sc} for a single junction device. If a device were grown such that the optimum dimensions were used an even larger short circuit current is anticipated.

6.4 Efficiency of Pm^{147} Battery

The efficiency of the single junction and multijunction devices is approximately 3% which is near the theoretical limit of 5% as discussed earlier. The efficiency is calculated by taking half the power output of the source since betas are emitted from both sides of the Pm^{147} source while the diode is only irradiated from one side and dividing it into the maximum power output obtained from the single and multijunction cells. The Pm^{147} source has a power output of 492 watts/cm^2 which yields efficiency of 2.94% for a single junction cell and 3.25% for a multijunction cell. This is considerably higher than the 1.85% efficiency reported by Olsen et al[8].

Although the devices evaluated in this investigation were only 1 cm^2 in area, no additional fabrication problems should be encountered in

constructing devices 3 or 4 cm^2 yielding 3 or 4 times the output power of a 1 cm^2 area device.

CHAPTER VII

CONCLUSION

The electron-voltaic effect in epitaxial P-N junctions has been investigated using the beta radiation emitted from a four curie source, 3 cm^2 in area, having a strength 2 mg/cm^2 of the radioisotope Pm^{147}. The power output of a single junction device 1 cm^2 in area has been evaluated and found to produce an open circuit voltage of 0.37 volts and a short circuit current of 29 μ amps, yielding a maximum power output of 7.2 μ watts and an efficiency of 2.94%. Multijunction devices which act as a two diodes in series have also been investigated and found to yield double the voltage (0.76V); near half the current (15.2 μ amp) of a single junction device; an increase in maximum power output of 11% (8.0 μ watts) and an increased efficiency to 3.25%. It is expected that for the optimum geometry of the multilayer device even a large increase in power output and efficiency can be achieved.

The silicon cells were evaluated for direct energy conversion using Pm^{147} as the beta source because it emits pure betas with a mean energy of 75 kev and a maximum energy of only 233 kev. Therefore the crystal damage due to the beta radiation should be small since most particles emitted are less than 200 kev, the damage threshold reported for silicon[5,6]. Also the half life of Pm^{147} is 2.6 years and therefore promethium should

provide a radioisotope source which can be used in conjunction with P-N junctions (in series or parallel combinations) to construct a small atomic battery with a relatively long lifetime (5-10 years). The performance of the battery should be limited by the lifetime of the Pm^{147} and not by the radiation damage of the semiconductor.

While both the single layer and multilayer devices yield similar output powers, the multijunction device would have an advantage for use in a battery which did not require a large current but did require a large voltage output. Less cells and therefore a decrease in size and the number of interconnections would be necessary for the construction of the battery using multilayer cells instead of single layer ones. The use of fewer interconnections should lead to an increased reliability of the atomic battery. A second advantage in the use of a multilayer structure should be found in its increased radiation resistance. The radiation damage of a single P-N junction cell is manifested in the minority carrier lifetime and thus diffusion length of minority carriers in the base region. In order to obtain large generation currents (i.e., I_{sc}) it is necessary to have long diffusion lengths. When these are reduced due to radiation damage so are the generation currents. In the multijunction devices the substrate receives a lower level of radiation than for a single junction device because of the layers of silicon between it and the Pm^{147} and therefore minority carrier lifetimes in this region are maintained longer. In the other P region of the multijunction device the collection efficiency is not much affected until the diffusion length becomes smaller than the

thickness of this region. Therefore the minority carrier lifetime may decrease appreciably before an effect is observed on I_{sc}. However, once the diffusion length is less than the thickness of the P region the deterioration in minority carrier lifetime and therefore short circuit current is similar to a single junction cell. Thus the multijunction cell should be superior in terms of lifetime caused by radiation damage to a single junction cell.

A possible use for the proposed atomic battery are as a source of biasing voltage for integrated circuits and even discrete solid state devices for cases in which a small long lived power supply is necessary as in space vehicles. A second use is as a power source for a cardiac pacemaker to be implanted under the skin with the pacemaker. Due to the low current but high voltage requirements of the electronics of the pacemaker the multijunction cells are more advantageous than single junction cells because they decrease the size of the battery which is needed and would likely have a longer lifetime.

Although the devices fabricated in this investigation were only 1 cm^2 in area, no additional problems should be encountered in constructing cells 3 or 4 cm^2 in area yielding 3 or 4 times the output power of a 1 cm^2 device. Also, devices with 3 and 4 active junctions should be able to be grown increasing V_{oc} by 3 and 4 times over a single junction device but cutting I_{sc} by 1/3 and 1/4 respectively.

APPENDIX A

SPREADING RESISTANCE MEASUREMENTS

The spreading resistance probe used in obtaining the doping profiles of the grown epitaxial layers was a model ASR-100 obtained from Solid State Measurements Inc. This type of probe measures the spreading resistance using one of two probes on the bevelled surface of the silicon wafer[25,32]. The value of spreading resistance obtained is then used to determine the resistivity of the sample. The sample is bevelled using a "Syton" polish obtained from Monsanto. The tangent of the bevel for most measurements was 0.02 and the probes took measurements at 5 micron steps. This results in 0.1 micron steps in the concentration profile. Once the spreading resistance profile is obtained the concentration profile is determined using a computor program supplied by Solid State Measurements Inc.

The program is shown below and contains correction factors when there is a P-N junction or insulating layer beneath the probe points. Mazur and Dickey[25] have shown that using two probes results in a better average value for the spreading resistance. For this reason, all measurements were conducted using two probes.

```
      PROGRAM TST (INPUT,OUTPUT,TAPE5=INPUT,TAPE6=OUTPUT)
    1 DIMENSION Y(30),G(30),H(30),M(30),K(30),R(200),V(30),P(30),NN
      INTEGER W,U,Z,PP
      REAL M,K2,K,N7
     CNUMBER OF SPREADING RESISTANCE CALIBRATION POINTS
     CAND THE DIFFERENCE BETWEEN SUBSEQUENT ITERATION
     CPOINTS IN THE CALCULATION (USUALLY.05)
    2 READ(5,3)N,E
    3 FORMAT(I2,F5.3)
     CSPREADING RESISTANCE CALABRATION DATA WRITTEN IN
     CTHE FORM, SPREADING RESISTANCE (OHMS),RESISTIVITY
     C N-TYPE(OHM-CM),RESISTIVITY P-TYPE(OHM-CM) LISTED
     C REPETITIVELY. THESE POINTS ARE TAKEN FROM A
     C CALABRATION CURVE  CONSTRUCTED FROM A SET STANDARDS
    4 READ(5,5)(Y(I),G(I),H(I),I=1,N)
    5 FORMAT(6E10.4)
     C PROBE DIAMETER(.0004) AND PROBE SPACING
    6 READ(5,7)A,D
    7 FORMAT(E10.4,F3.1)
     C CARRIER CONCENTRATION CORRESPONDING TO THE
     C RESISTIVITY OF THE G(I) AND H(I)
    8 READ(5,9)(V(I),P(I),I=1,N)
    9 FORMAT(8E8.3)
     C SAMPLE IDENTIFICATION NUMBER
   10 READ(5,11)SID
   11 FORMAT(A7)
      CALL LETTER(7,0.12,270.,6.5,5.5,SID)
     C TANGENT OF THE BEVEL,NUMBER OF PROBES USED,
     C X-STEP OF THE PROBES
   12 READ(5,131)TL,PP,X
  131 FORMAT(E6.4,I1,E6.4)
     C LAYER NUMBER,JUNCTION DEPTH,LAYER TYPE(1 FOR N - 2
     C FOR P), NUMBER OF SPREADING RESISTANCE DATA POINTS
     C IN LAYER
   14 READ(5,15)L7,Q,U,W,Z
   15 FORMAT(I1,F10.5,I1,I3,I1)
   16 IF(Z.EQ.1)GO TO 21
   17 WRITE(6,18)L7,Q,U,W
   18 FORMAT(25H NEXT LAYER L7,Q,U,W ARE ,I4,1PE14.5,I3,I4)
   19 GO TO 27
   21 WRITE(6,22)SID
   22 FORMAT(1H1,13HSAMPLE ID IS ,A7)
      WRITE(6,26)A,D,TL,PP,X
   26 FORMAT(17H A,D,TL,PP,X ARE ,F10.5,F3.1,F6.4,I3,F6.4//
     1  6X,13HMEASURED      ,12HDEPTH        ,13HRESISTIVITY
     2  13HNET DOPANT    ,5HPOINT/14H SPR.RES.      ,12H
     3  13H              ,13H DENSIYY       ,5H NO. /14H  (OHMS)
     4  12H(MICRONS)     ,13H  (OHM-CM     ,13H(PER CM-3)    //)
   27 IF(L7=50.0)GO TO 200
   28 IF(U.EQ.2)GO TO 35
   30 DO 31 I=1,N
   31 M(I)=G(I)
   34 GO TO 39
   35 DO 36 I=1,N
   36 M(I)=H(I)
```

```
 39 DO 40 I=1,N
 40 K(I)=2.0*A*M(I)/Y(I)
 C SPREADING RESISTANCE DATA
 50 READ(5,55)(R(J),J=1,W)
 55 FORMAT(10E6.3)
 59 DO 260 J=1,W
 60 T=0-((J-1)*X*TL)
 65 IF(T.LE.0.0)GO TO 80
 70 C=1+2.0*A*(ALOG(D/(2.0*T))-0.116)/(3.141593*T)
 75 GO TO 85
 80 C=1.0
 85 T1=((4.0*A)/FLOAT(PP))*R(J)
 90 DO 95 I=1,N
 94 IF(R(J).LE.M(I))GO TO 105
 95 CONTINUE
105 T2=(ALOG(Y(I))-ALOG(Y(I-1)))*(ALOG(R(J))-ALOG(M(I-1)))
110 B2=ALOG(M(I))-ALOG(M(I-1))
115 Y2=EXP(ALOG(Y(I-1))+T2/B2)
120 DO 130 I=1,N
125 IF(ALOG(Y2).LE.ALOG(Y(I)))GO TO 135
130 CONTINUE
135 T3=(K(I)-K(I-1))*(ALOG(Y(I))-ALOG(Y2))
140 B3=ALOG(Y(I))-ALOG(Y(I-1))
145 K2=K(I)-T3/B3
150 IF(ABS(T1/(K2-1+C)-Y2).LE.(E*Y2))GO TO 160
151 Y2=T1/(K2-1+C)
155 GO TO 120
160 IF(J.GT.1)GO TO 170
165 S7=0
170 S7=S7+(X*TL)/Y2
171 RS7=1/S7
175 IF(U.GE.2)GO TO 225
180 DO 200 I=1,N
185 IF(Y2.LE.Y(I))GO TO 205
200 CONTINUE
205 T4=(ALOG(V(I))-ALOG(V(I-1)))*(ALOG(Y2)-ALOG(Y(I-1)))
210 B4=ALOG(Y(I))-ALOG(Y(I-1))
215 N7=EXP(ALOG(V(I-1))+T4/B4)
220 GO TO 256
225 DO 240 I=1,N
230 IF(Y2.LE.Y(I))GO TO 245
240 CONTINUE
245 T5=(ALOG(P(I))-ALOG(P(I-1)))*(ALOG(Y2)-ALOG(Y(I-1)))
250 B5=ALOG(Y(I))-ALOG(Y(I-1))
255 N7=EXP(ALOG(P(I-1))+T5/B5)
256 QT=(Q-T)*40000.
    IF(L7.GT.1) GO TO 257
    YDIST=-(QT)
    SUM=YDIST
    GO TO 258
257 YDIST=SUM-(X*TL*40000.)-QT
    IF(J.LT.W) GO TO 258
    SUM=YDIST
258 XDIST=ALOG10(N7)
    IF(LL.EQ.13) GO TO 888
    XX=1.0*(XDIST-13.0)-1.0
    GO TO 890
888 XX=1.0*(XDIST-13.0)+1.0
890 YY=YDIST/2.+6.0
```

```
  260 WRITE(6,265)R(J),QT,Y2,N7,J
  265 FORMAT(F13.0,F12.5,1P2E13.5,I5)
  266 WRITE(6,270)L7,0,U,W
  270 FORMAT(14H L7,0,U,W ARE ,I4,1P2E14.5,2I5)
  275 WRITE(6,280)RS7
  280 FORMAT(32H CALCULATED SHEET RESISTANCE IS ,F8.3)
  285 GO TO 14
  290 STOP
      END
     C EXAMPLE OF INPUT DATA
21 0.05
0.0005     2.5        0.97       0.001      4.6        1.9
0.002      8.3        3.8        0.005      18.0       8.3
0.01       33.5       18.0       0.02       80.0       42.5
0.05       215.0      121.0      0.1        430.0      265.0
0.2        745.0      470.0      0.5        2000.0     1150.0
1H0        4900.0     2600.0     2.0        7400.0     4600.0
5.0        17000.0    10700.0    10.0       33000.0    23000.0
20.0       86000.0    51000.0    50.0       195000.0   140000.0
100.0      295000.0   310000.0   200.0      450000.0   665000.0
500.0      780000.0   1900000.0  1000.0     1080000.0  4050000.0
2000.0     1800000.0  8000000.0
0.00040    0.1
  2.0E20   2.0E20   8.3E19   1.0E20   3.7E19   6.2E19 1.32E19   2.4E19
  5.0E18 1.15E19   1.5E18   5.0E18 2.75E17   1.5E18   8.8E16   5.0E17
  3.6E16 1.65E17 1.23E16   4.1E16   5.4E15   1.6E16   2.5E15   7.0E15
  9.8E14 2.75E15   4.9E14 1.35E15   2.5E14   6.8E14   1.0E14 2.75E14
  5.2E13   1.4E14   2.6E13   7.0E13 1.05E13   2.8E13   5.3E12   1.4E13
  2.6E12   7.0E12
1521
0 4
EG 104D
0H023 20.0005
1 0.000065 1  61
 8.8E11.06E21.23E21.60E22.65E26.65E2
2  0.00     2 102
4H35E3 3.5E3 3.9E3 4.0E33.75E33.75E3 3.8E3 3.4E33.85E33.85E3
0  0.0      0 00
*           END OF FILE
```

CD TOT 0157

APPENDIX B

HALL EFFECT MEASUREMENTS

The Hall effect measurements used to determine the mobility and average resistivity of a grown layer were determined by the method of Van der Pauw[27]. The clover leaf patterns were formed on the layer surface by evaporating a thick (> 10,000 Å) layer of aluminum through a clover leaf shadow mask onto the sample surface. Aluminum is evaporated onto the back surface. Black wax dots, approximately 20 mils. in diameter, were then deposited onto the ends of the clover leaves and over the entire back surface. The sample was then etched in an $HF-HNO_3$ (1:20) solution using the aluminum as a mask. After etching the aluminum is stripped off, except under the wax dots, using a hot solution of phosphoric, acetic, and nitric acids (25:5:3). The wax is then removed using chloroform. The sample is immediately rinsed in alcohol and blown dry in helium.

Next the sample is tested on a curve tracer to determine whether or not the mesa structure behaves as a rectifier and that the reverse leakage current is less than 1% of the conductivity current of the layer to ensure that the measurements to be performed are isolated in the layer and are not appreciably effected by the substrate. The sheet resistivity is determined by passing a known current through two adjacent leaves and measuring the voltage developed across the remaining two. The current chosen was one which resulted in a voltage of 50 mv. The sheet resistivity

is given by[27]

$$\rho = (\pi/\ln^2)\ (V/I)$$

The sheet Hall coefficient was measured by placing the sample in a magnetic field of 5 kgaus such that the field was perpendicular to the junction. A current (the same magnitude as that used to determine the sheet resistivity) was passed through two opposite leaves and measuring the voltage resulting across the remaining two. The magnetic field is then reversed and the voltage is measured once more. Using the change in voltage due to the change in direction of the magnetic field, the sheet Hall coefficient R_H may be determined[27]

$$R_H = 10^8\ (\Delta V/2\ /\ BI)$$

The Hall mobility is given by:

$$\mu_H = \frac{R_H}{\rho}$$

and the average doping density in the layer is given by $N = 6.25 \times 10^{18} / qt \times R_H$ [27] where t is the layer thickness.

APPENDIX C

Fabrication of Mesa Diodes

After the epitaxial layers had been grown metal contacts were evaporated into the top and bottom of the sample. The base pressure in the evaporator (an NRC 3116 Vacuum Coater) before evaporation was less than 4×10^{-6} torr. The contact to the P-type base region was 3000 Å of Al, which covered the entire back surface. On the N^+ surface first 500 Å of Ti and then 1400 Å of Ag was deposited through a circular mask leaving a dot slightly less than 1 cm^2 in area. The sample was then sintered at 450°C in a vacuum less than 4×10^{-6} torr, for 10 minutes. This procedure gives low resistivity (< 0.5 Ω) contacts[33]. It should be noted however that for construction of cells for battery applications a layer of Pd should be deposited between the Ti and the Ag to prevent moisture from corroding the Ti-Ag contact thus increasing the resistance of the contact and destroying its adhesion to the silicon. Some diodes were also constructed with contacts of 2000 Å of Al to the N^+ surface and the contacts not sintered.

Next the top contact was covered with a circular black wax dot by placing a mask made of 0.003" brass with a circular hole 1 cm^2 in area over the heated substrate and pressing the wax onto the substrate through the mask. The temperature of the substrate must not be too hot or the wax will run under the mask and yield a non-uniform pattern. The base area is completely covered with wax. The sample is then etched well into the substrate in a solution of HNO_2-HF (20:1) which etches the exposed silicon at a rate of 0.8 microns/minute.

After etching the device is rinsed in deionized water and blown dry in helium. Then the wax is stripped off in chloroform; the sample rinsed in alcohol and finally blown dry in helium. It should be noted that the mesa structures so formed were not passivated.

APPENDIX D

I-V CHARACTERISTICS

In order to measure the I-V characteristics of mesa diodes the device was placed in a light-tight box and mounted on a plate which made an electrical contact to the bottom of the device. Contact to the top was made by a needle probe. The dark current I-V characteristics were then measured point by point using a variable voltage supply (Harrison 6206B D.C. power supply purchased from Hewlett Packard) in parallel with the device and an ammeter (keithley 419 Picoammeter) in series.

Once the dark current I-V characteristics were obtained the device was placed inside a glove box containing the Pm^{147} beta source. The source was four curies of promethium oxide 0.75" in diameter evaporated onto a 1" diameter stainless steel disk. The source strength then is 2 mg /cm^2 using a specific activity for promethium oxide of 680 ci/gm.[8]

The source and sample were mounted as shown in Figure D-1. The top of the mesa was separated from the radioisotope by 0.001" aluminum wire which served as the contact to the irradiated side of the diode. The variable resistance shown in Figure D-1 is a resistance box having a range from 100 Ω to 10 MΩ. Using the known value of resistance and the voltage across the device terminals measured by the DVM one may determine I_{sc}, V_{oc} and any other point on the I-V curve for the irradiated diode. Thus one obtains a point by point I-V curve of the irradiated diode from which one

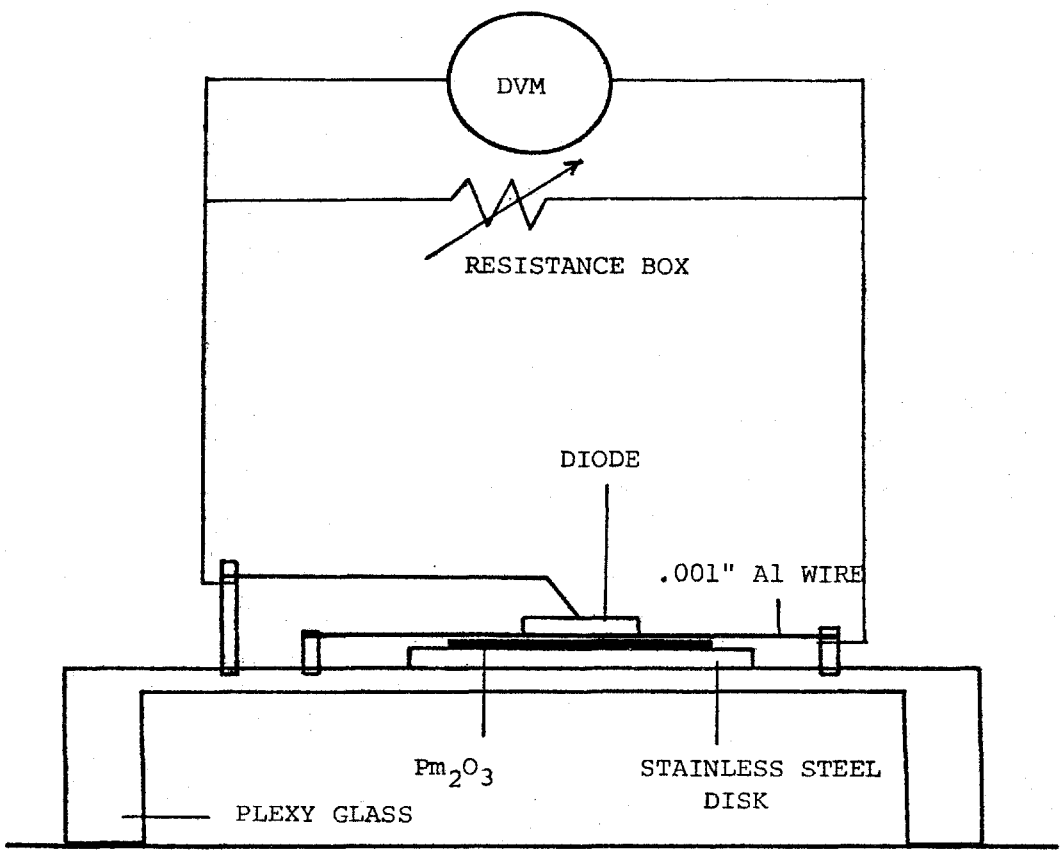

Figure D-1 Schematic for the diode evaluation when irradiated by the beta particles emitted from the promethia source (2 mg/cm^2).

may determine the power output available from the device.

APPENDIX E

Calculation of the Optimum Geometry for a Multijunction Device

Using the theory outlined in Section3.3 the computer program below was used to determine the optimum geometry for a two diode in series multijunction device by employing Gaussian reduction. the following values were used in the numerical calculations.

Intrinsic carrier concentration= 1.5×10^{16} cm^{-2}

Incident flux of 4 Ci source = $6.25 \times 10^{18} cm^{-2}\text{-}sec^{-1}$

Si absorption coefficient = 4×10^{4} m^{-1}

Doping density p-type = 1×10^{22} m^{-3}

Doping density N^{+} and P^{+} = 1×10^{25} m^{-3}

τ_n = 3×10^{-6} sec

τ_p and τ_n (P^{+} layer) = 1×10^{-7} sec

Diffusion coefficient P-layer = .0025 cm^2/sec

Diffusion coeficient P^{+}-layer = .002 cm^2/sec

Diffusion coefficient N^{+}-layer = .001 cm^2/sec

Conductance of tunnel diode = 1×10^{4} mho

```
      COMMON/B1/A(9,11),X(10)
      REAL NO2,NO4,N1,N2,N3,N4,N5,NX,NO3,NO5
C READ INTRINSIC DOPING LEVEL,BETA FLUX,BETA ABSORBTION
C COEFFICIENT FOR SI ,CONDUCTANCE OF P+N+ TUNNEL DIODE
111   READ 10,TN,THI,ALP,GTUN
      IF(TN.LE.0.0) STOP
C DEPTHS OF LAYERS FROM SURFACE
      READ 10,X1,X2,X3,X4,X5
C DOPING DENSITIES OF EACH LAYER
      READ 10,D1,D2,D3,D4,D5
C MINORITY CARRIER LIFETIMES OF EACH LAYER
      READ 10,T1,T2,T3,T4,T5
C MINORITY CARRIER DIFFUSION LENGTHS
      READ 10,DC1,DC2,DC3,DC4,DC5
 10   FORMAT(10F8.3)
C CALCULATE CARRIER CONCENTRATIONS IN LAYERS
      PO1=TN*TN/D1
      NO2=TN*TN/D2
      NO3=TN*TN/D3
      PO4=TN*TN/D4
      NO5=TN*TN/D5
C CALCULATE MINORITY CARRIER DIFFUSION LENGTHS
      DL1=SQRT(T1*DC1)
      DL2=SQRT(T2*DC2)
      DL3=SQRT(T3*DC3)
      DL4=SQRT(T4*DC4)
      DL5=SQRT(T5*DC5)
C CALCULATE SEVERAL TERMS WHICH ARE CONSTANT
C ONCE THE GEOMETRY IS CHOSEN
      EP1=EXP(X1/DL1)
      EP3=EXP(X3/DL4)
      EP4=EXP(X4/DL4)
      EN1=EXP(X1/DL2)
      EN2=EXP(X2/DL2)
      ENX=EXP(X2/DL3)
      EN3=EXP(X3/DL3)
      EN4=EXP(X4/DL5)
      EN5=EXP(X5/DL5)
      A1=EXP(-ALP*X1)
      A2=EXP(-ALP*X2)
      A3=EXP(-ALP*X3)
      A4=EXP(-ALP*X4)
      A5=EXP(-ALP*X5)
      B1=1.-1./(ALP*ALP*DL1*DL1)
      B2=1.-1./(ALP*ALP*DL2*DL2)
      B3=1.-1./(ALP*ALP*DL3*DL3)
      B4=1.-1./(ALP*ALP*DL4*DL4)
      B5=1.-1./(ALP*ALP*DL5*DL5)
C TOTAL ELECTRON -HOLE PAIRS GENERATED IN INFINITELY
C THICK SEMICONDUCTOR
      CT=1.6E-19*THI
C CORRECTION DUE TO FINITE LENGTH OF SEMICONDUCTOR
      CP=CT*(1.-A5)
      PRINT 2,TN,THI,ALP,GTUN,CT,CP
  2   FORMAT(1H1,*ANALYSIS OF 5 LAYER DIODE (NPPNP)*/
     11H *INTRIN.CONC.=*E12.2*    THI,ALP =*2E12.2/
     51H *TUNNEL CONDUCTANCE =*E12.2/
     21H *POSSIBLE GEN CURRENT AND CURRENT ABS. IN SEMI =*2E12.2/
     31H0,24X,*REGION 1    REGION 2    REGION 3    REGION 4    REGION
```

```
   4)
    PRINT 3,X1,X2,X3,X4,X5,D1,D2,D3,D4,D5,T1,T2,T3,T4,T5,DC1,DC2,
   1DC3,DC4,DC5,DL1,DL2,DL3,DL4,DL5
 3  FORMAT(1H0,*MAX.DISTANCE*,8X,5E12.2/1H ,*DOPING*14X,5E12.2/
   11H ,*LIFETIMES*11X,5E12.2/1H ,*DIFF.CONSTANT*7X,5E12.2/
   21H ,*DIFF.LENGTHS*8X,5E12.2/1H0,22X,*JUNCTION 0  JUNCTION 1  JUNC
   3TION 2  JUNCTION 3  JUNCTION 4  JUNCTION 5*)
    DO 20 I=1,9
    DO 20 J=1,11
   C PUT COEFFICIENTS OF UNKNOWNS IN ARRAY
20  A(I,J)=0.0
    A(6,1)=EP4
    A(6,2)=1./EP4
    A(6,5)=-D5*EN4/D4
    A(6,6)=-D5/(D4*EN4)
    A(6,11)=     THI*A4/(ALP*DC4*B4)              -D5*THI*A4/(D4*ALP*DC5*E
   1)
    A(2,1)=DC4*EP4/DL4
    A(2,2)=-DC4/(EP4*DL4)
    A(2,3)=-DC1*EP1/DL1
    A(2,4)=DC1/(EP1*DL1)
    A(2,5)=-DC5*EN4/DL5
    A(2,6)=DC5/(EN4*DL5)
    A(2,7)=DC2*EN1/DL2
    A(2,8)=-DC2/(EN1*DL2)
    A(2,11)=-THI*A1/B2+THI*A1/B1+THI*A4/B5-THI*A4/B4
    A(3,3)=1.0
    A(3,4)=1.0
    A(3,11)=THI/(ALP*DC1*B1)
    A(4,3)=EP1
    A(4,4)=1./EP1
    A(4,7)=-D2*EN1/D1
    A(4,8)=-D2/(D1*EN1)
    A(4,11)=     THI*A1/(ALP*DC1*B1)              -D2*THI*A1/(D1*ALP*DC2*E
   1)
    A(5,5)=EN5
    A(5,6)=1./EN5
    A(5,11)=THI*A5/(ALP*DC5*B5)
    A(1,1)=EP3
    A(1,2)=1./EP3
    A(1,9)=-D3*EN3/D4
    A(1,10)=-D3/(D4*EN3)
    A(1,11)=     THI*A3/(ALP*DC4*B4)              -D3*THI*A3/(D4*ALP*DC3*E
   1)
    A(9,1)=EP3*DC4/DL4
    A(9,2)=-DC4/(EP3*DL4)
    A(9,3)=-EP1*DC1/DL1
    A(9,4)=DC1/(EP1*DL1)
    A(9,7)=DC2*EN1/DL2
    A(9,8)=-DC2/(EN1*DL2)
    A(9,9)=-DC3*EN3/DL3
    A(9,10)=DC3/(DL3*EN3)
    A(9,11)=-THI*A1*(1./B2-1./B1)+THI*A3*(1./B3-1./B4)
    A(7,7)=EN2
    A(7,8)=1./EN2
    A(7,9)=-D3*EN3/D2
    A(7,10)=-D3/(EN3*D2)
    A(7,11)=THI*A2/(ALP*DC2*B2)-THI*A2*D3/(ALP*D2*DC3*B3)
    A(8,7)=EN2*DC2/DL2
```

```
      A(8,8)=-DC2/(EN2*DL2)
      A(8,9)=-ENX*DC3/DL3
      A(8,10)=DC3/(ENX*DL3)
      A(8,11)=-THI*A2/B2+THI*A3/B3
      CALL GASS
     C READTUNNEL DIODE BIAS(POINT FROM WHICH THE CALCULATION
     C OF VOC AND ISC BEGINS),SEARCH STEP(INITIAL)+A GATING PARAMETER,
     C OF VOC AND ISC BEGINS),SEARCH STEP(INITIAL)+A GATING
     C PARAMETER,ACCURACY PARAMETER+GATING PARAMETER
  100 READ 10,V3,DV,CSC
      IF(V3.GT.100.) GO TO 111
      IC=0
  101 N3=NO3*EXP(V3/0.02586)
      TP=EN3/A(9,9)
      CTUN=GTUN*V3
      ATUN=A(9,11)+CTUN/1.6E-19
      X(10)=(N3-NO3+THI*A3/(ALP*DC3*B3)-TP*ATUN    )/(1./EN3-TP*A(9,10))
      DO 40 I=1,9
      IM=10-I
      IP=IM+1
      SUM=0.0
      IF(IM.EQ.9) SUM=-CTUN/1.6E-19
      DO 50 J=IP,10
   50 SUM=SUM+X(J)*A(IM,J)
      X(IM)=(A(IM,11)-SUM)/A(IM,IM)
   40 CONTINUE
      CP0=1.6E-19*(-X(3)*DC1/DL1+X(4)*DC1/DL1-THI/B1)
      CP1=1.6E-19*(-X(3)*DC1*EP1/DL1+X(4)*DC1/(DL1*EP1)-THI*A1/B1)
      CP3=1.6E-19*(-X(1)*DC4*EP3/DL4+X(2)*DC4/(DL4*EP3)-THI*A3/B4)
      CP4=1.6E-19*(-X(1)*DC4*EP4/DL4+X(2)*DC4/(DL4*EP4)-THI*A4/B4)
      CN1=1.6E-19*(X(7)*DC2*EN1/DL2-DC2*X(8)/(DL2*EN1)+THI*A1/B2)
      CN2=1.6E-19*(X(7)*DC2*EN2/DL2-DC2*X(8)/(DL2*EN2)+THI*A2/B2)
      CN4=1.6E-19*(X(5)*DC5*EN4/DL5-DC5*X(6)/(DL5*EN4)+THI*A4/B5)
      CN5=1.6E-19*(X(5)*DC5*EN5/DL5-DC5*X(6)/(DL5*EN5)+THI*A5/B5)
      CNX=1.6E-19*(X(9)*DC3*ENX/DL3-DC3*X(10)/(DL3*ENX)+THI*A2/B3)
      CN3=1.6E-19*(X(9)*DC3*EN3/DL3-DC3*X(10)/(DL3*EN3)+THI*A3/B3)
      P0=P01+X(3)+X(4)-THI/(ALP*DC1*B1)
      P1=P01+X(3)*EP1+X(4)/EP1-THI*A1/(ALP*DC1*B1)
      P3=P04+X(1)*EP3+X(2)/EP3-THI*A3/(ALP*DC4*B4)
      P4=P04+X(1)*EP4+X(2)/EP4-THI*A4/(ALP*DC4*B4)
      N1=NO2+X(7)*EN1+X(8)/EN1-THI*A1/(ALP*DC2*B2)
      N2=NO2+X(7)*EN2+X(8)/EN2-THI*A2/(ALP*DC2*B2)
      N4=NO5+X(5)*EN4+X(6)/EN4-THI*A4/(ALP*DC5*B5)
      N5=NO5+X(5)*EN5+X(6)/EN5-THI*A5/(ALP*DC5*B5)
      NX=NO3+X(9)*ENX+X(10)/ENX-THI*A2/(ALP*DC3*B3)
      IF(N1.LE.0.0) GO TO 112
      IF(N2.LE.0.0) GO TO 112
      IF(N3.LE.0.0) GO TO 112
      IF(N4.LE.0.0) GO TO 112
      IF(N5.LE.0.0) GO TO 112
      IF(NX.LE.0.0) GO TO 112
      V1=0.02586*ALOG(N1/NO2)
      V2=0.02586*ALOG(N2/NO2)
      V3=0.02586*ALOG(N3/NO3)
      V4=0.02586*ALOG(N4/NO5)
      VA=V1-V3+V4
      PRINT 5,VA,V1,V2,V3,V4,CP0,CP1,CP3,CP4,CN1,CN2,CN3,CN4,CN5,CNX,
     1P0,P1,P3,P4,N1,N2,N3,N4,N5,NX,CTUN
    5 FORMAT(1H0,*   SOLUTION AT *E12.2*  VOLTS*/1H0*FERMI DIFFERENCE*
```

```
      116X,4E12.2/1H0,*CURRENT P*11X,2E12.2,12X,2E12.2/1H *CURRENT N*23X
      25E12.2/1H ,44X,E12.2/
      31H0*HOLE CONC.*10X,2E12.2,12X,2E12.2/1H *ELECTRON CONC.*18X,5E12.
      4/1H ,44X,E12.2/1H * CTUN=*E12.2)
       IF(DV.NE.0.0) GO TO 114
       GO TO 100
  112  PRINT 113
  113  FORMAT(1H *NO SOLUTION AT THIS V3*)
       PRINT 130,N1,N2,N3,N4,N5,NX
  130  FORMAT(1H ,12X,5E12.2/1H ,24X,E12.2)
       IF(IC.GT.50) GO TO 118
       DV=DV/2.
       IF(DV.NE.0.0) V3=V3+DV
       IF(DV.NE.0.0) IC=IC+1
       IF(DV.NE.0.0) GO TO 101
       GO TO 100
  114  DV=DV/2.
       IF(CSC.GT.0.0) GO TO 117
       IF(ABS(VA).LT.0.001) GO TO 115
       V3=V3-   DV*VA/ABS(VA)
       GO TO 118
  117  CD=CP1+CN1
       IF(ABS(CD).LE.CSC) GO TO 115
       V3=V3+DV*CD/ABS(CD)
  118  IC=IC+1
       IF(IC.LT.51) GO TO 101
       PRINT 116,V3,DV
  116  FORMAT(1H0*DIVERGED  -  V3,DV =*E12.8,E12.2)
  115  DV=0.0
       GO TO 100
       END
       SUBROUTINE GASS
       COMMON/B1/A(9,11),X(10)
       DO 10 I=1,8
       IP=I+1
       DO 20 K=IP,9
       TP=A(K,I)/A(I,I)
       IF(TP.EQ.0.0) GO TO 20
       A(K,I)=0.0
       DO 30 J=IP,11
   30  A(K,J)=A(K,J)-TP*A(I,J)
   20  CONTINUE
   10  CONTINUE
       RETURN
        END
         6400 END OF RECORD
     C SAMPLE OF DATA
  1.5E16 6.25E18     4.E4     1.E4
   5.E-7 1.42E-5 1.47E-5 1.52E-52.652E-4
   1.E25    1.E22    1.E25    1.E25    1.E22
   1.E-7    3.E-6    1.E-7    1.E-7    3.E-6
0.001     0.0025  0.002    0.001    0.0025
-1.0
-0.5
 0.2
-0.1
-0.07
-0.06
-0.05
```

```
-0.04
-0.03
-0.02
-0.01
0.0
0.1
0.2
0.3
0.4
0.5
0.6
0.7
0.8
0.9
0.0       -0.0001
0.0       -0.0001      1.E-4
9
```

REFERENCES

1. P. Rappaport, Phys. Rev., 93, 246 (1953).
2. W. G. Pfann and W. van Roosbroeck, J. Appl. Phys., 25, 1422 (1954).
3. P. Rappaport, J. J. Loferski and E. G. Linder, R.C.A. Rev., 17, 100, March (1956).
4. H. Flicker, J. J. Loferski and T. S. Elleman, IEEE Trans. on El. Dev., 11, 2 (1964).
5. H. Flicker, J. J. Loferski and J. Scott-Monck, Phys. Rev., 128, 2557 (1962).
6. R. L. Novack, Bull. Am. Phys. Soc., (2) 8, 235 (1963).
7. T. L. Chu and G. A. Gruber, J. Electrochem. Soc., 114, 522 (1967).
8. Larry C. Olsen, Stephen E. Seeman, Bobby I. Griffin and Charles J. Ambrose, United States Patent 3,706,893, December 19, 1972.
9. J. P. McKelvey, "Solid State and Semiconductor Physics", Harper and Row, New York (1966).
10. S. N. Sze, "Physics of Semiconductor Devices", Wiley-Interscience, New York (1969).
11. K. G. McKay and K. B. McAfee, Phys. Rev., 91, 1079 (1952).
12. C. Bussolati, A. Fiorentini and G. Fabri, Phys. Rev., 136, A1756 (1964).
13. V. S. Vavilov, "Effects of Radiation on Semiconductors", Consultants Bureau, New York (1965).
14. M. Wolf, Proceedings of the I.R.E., __, 1246 (1960).
15. Robert W. Rostron, IEEE Trans. on El. Dev., 19, 1024 (1972).

16. M. Wolf, Energy Conversion, 11, 63 (1971).

17. M. Wolf and H. Rauschenbach, Energy Conversion, 3, 455 (1963).

18. A. R. Sattler and F. L. Vook, Phys. Rev., 155, 211 (1967).

19. S. R. Bhola and A. Mayer, R.C.A. Rev., 24, 511 (1963).

20. D. Richman and R. H. Arlett, "Semiconductor Silicon"; R. R. Hanerecht and E. L. Kern, eds, p. 200, Electrochemical Society, New York, May 1969.

21. W. Kern and D. Puotinen, R.C.A. Rev., 31, 187 (1970).

22. E. Sirth and A. Adler, Z. Metallk, 52, 529 (1961).

23. Y. S. Chiang and D. Richman, Met. Trans., 2, 743 (1971).

24. D. C. Gupta, Solid State Technology, 14, 33 (1971).

25. R. G. Mazur and D. H. Dickey, J. Electrochem. Soc., 113, 255 (1966).

26. L. J. van der Pauw, Philips Res. Repts., 13, 1 (1958).

27. R. V. Babcock, J. Electrochem. Soc., 108, 1119 (1961).

28. Philip F. Kane and Graydon B. Larrabee, "Characterization of Semiconductor Materials", McGraw-Hill, New York (1970).

29. U.S. Government Report, ASD-TDR-63-376, Vol. V.

30. P. Rai Choudbury and E. I. Salkovitz, J. Cryst. Growth, 7, 353 (1970).

31. S. R. Lederhandler and L. J. Giacoletto, Proc. I.R.E., 43, 477 (1955).

32. R. G. Mazur, J. Electrochem. Soc., 114, 255 (1967).

33. F. Fischer and R. Geretch, Extended Abstracts, Electrochem. Soc., Spring Meeting, p. 294, May 1969.

34. R. Lenie, S. C. P. and Solid State Tech., 7, 41 (1964).

35. J. P. Mize and W. R. Runyan, "Metallurgy of Advanced Electronic Materials", Geoffrey E. Brock, ed., Interscience Publishers, New York (1963).

36. T. J. Rogers and J. D. Meindl, IEEE on El. Dev., 20, 226 (1973).

37. R. A. Sunshine and J. Assoun, Solid State Electronics, 16, 459 (1973).

38. W. Shockley, Solid State Electronics, 2, (1961).